NAR Cancer, 2024, **6**, 1–22
https://doi.org/10.1093/narcan/zcae003
Advance access publication date: 29 January 2024
DNA Damage Sensing and Repair

The ORFIUS complex regulates ORC2 localization at replication origins

Zelei Yang[1], Saie Mogre[1], Ruiyang He[1], Emma L. Berdan[2], Shannan J. Ho Sui[2] and Sarah J. Hill[1,3,*]

[1]Department of Medical Oncology and Division of Molecular and Cellular Oncology, Dana-Farber Cancer Institute, Boston, MA 02215, USA
[2]Harvard Chan Bioinformatics Core, Harvard T.H. Chan School of Public Health, Boston, MA 02115, USA
[3]Harvard Medical School, Boston, MA 02115, USA

[*]To whom correspondence should be addressed. Tel: +1 617 632 4269; Fax: +1 617 582 8601; Email: Sarah_hill@dfci.harvard.edu

Abstract

High-grade serous ovarian cancer (HGSC) is a lethal malignancy with elevated replication stress (RS) levels and defective RS and RS-associated DNA damage responses. Here we demonstrate that the bromodomain-containing protein BRD1 is a RS suppressing protein that forms a replication origin regulatory complex with the histone acetyltransferase HBO1, the BRCA1 tumor suppressor, and BARD1, ORigin FIring Under Stress (ORFIUS). BRD1 and HBO1 promote eventual origin firing by supporting localization of the origin licensing protein ORC2 at origins. In the absence of BRD1 and/or HBO1, both origin firing and nuclei with ORC2 foci are reduced. BRCA1 regulates BRD1, HBO1, and ORC2 localization at replication origins. In the absence of BRCA1, both origin firing and nuclei with BRD1, HBO1, and ORC2 foci are increased. In normal and non-HGSC ovarian cancer cells, the ORFIUS complex responds to ATR and CDC7 origin regulatory signaling and disengages from origins during RS. In *BRCA1*-mutant and sporadic HGSC cells, BRD1, HBO1, and ORC2 remain associated with replication origins, and unresponsive to RS, DNA damage, or origin regulatory kinase inhibition. ORFIUS complex dysregulation may promote HGSC cell survival by allowing for upregulated origin firing and cell cycle progression despite accumulating DNA damage, and may be a RS target.

Graphical abstract

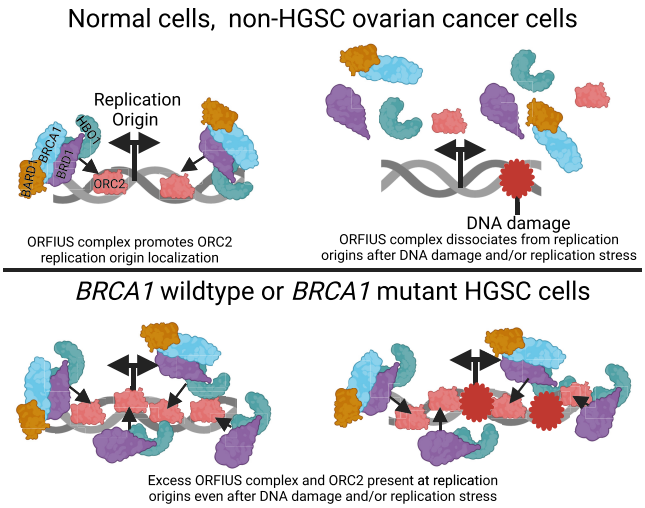

Introduction

High-grade serous ovarian cancer (HGSC) is a lethal malignancy, with 70% of patients succumbing to their disease within five years of diagnosis (1). Limited therapies beyond chemotherapy and surgery exist (1). Genomic analyses suggest that many HGSCs may have either (i) increases in, and/or (ii) defects in the response to replication fork slowing or stalling, which is currently broadly referred to as replication stress (RS), making RS therapies additional options (2–5).

The mechanistic understanding of responding to and targeting RS is a rapidly evolving field (3–5). There are many sources of RS in HGSC including but not limited to unrepaired DNA damage which blocks fork progression, and RS can be exacerbated by many factors such as dysregulated replication origin firing (3,4). Once a replication fork stalls, the RS response led

Received: April 10, 2023. **Revised:** December 18, 2023. **Editorial Decision:** January 4, 2024. **Accepted:** January 9, 2024
© The Author(s) 2024. Published by Oxford University Press on behalf of NAR Cancer.
This is an Open Access article distributed under the terms of the Creative Commons Attribution-NonCommercial License (http://creativecommons.org/licenses/by-nc/4.0/), which permits non-commercial re-use, distribution, and reproduction in any medium, provided the original work is properly cited. For commercial re-use, please contact journals.permissions@oup.com

by the ATR kinase is activated to help stabilize and restart the fork (3). If a stalled fork is not stabilized or restarted, the replication machinery can be misplaced on or separated from the DNA and the fork can collapse, potentially causing DNA damage (3–5). The majority of HGSCs harbor alterations in (i) DNA damage repair (DDR) genes, particularly in *BRCA1* stalled replication fork protection pathways, which may cause repair defects which both increase fork stalling and prevent stabilization, restart, or repair of stalled or possibly collapsed forks; and/or (ii) alterations in cell cycle regulatory genes like *RB1* or *TP53,* or oncogenes like *CCNE1*, which can increase or exacerbate RS by causing defective cell cycle checkpoints or altering S phase entry or progression (2,6,7). HGSCs harboring such genomic alterations may have increased basal RS and/or defects in responding to RS and therefore be more sensitive to therapies which stall forks, such as carboplatin or PARP inhibitors (PARPi), or block the RS response, such as ATR inhibitors, amongst others (2). However, only some HGSC patients respond to RS therapies, and even those who do respond develop resistance (1,8–10). Additional RS therapies are needed.

There has recently been a focus on targeting bromodomain (BRD)-containing proteins in HGSC, because, amongst their many diverse functions in transcription and chromatin modification, they have multiple roles in preventing or modulating the response to RS (11). The BRD and extra-terminal domain (BET) family of BRD-containing proteins, in particular BRD4, is most heavily studied in this regard. BRD4 inhibition has been shown to sensitize HGSC cells to RS-inducing PARPis through transcriptional downregulation of DDR pathways (12–14). In addition, BRD4 inhibition can directly lead to RS by causing DNA/RNA hybrid (R loop) formation which creates obstacles in the DNA and causes replication/transcription collisions (15).

Given these promising results with BRD4, it is exciting that there are at least 42 known human BRD-containing proteins, many of which are structurally unrelated to BRD4 (11). Most non-BET BRD-containing proteins have as yet unstudied roles in replication or the RS response and may represent novel therapeutic targets in HGSC with distinct functions (11). Given this possibility, in an attempt to expand the targetable BRD-containing protein repertoire in HGSC, we focused here on the non-BET BRD-containing protein BRD1 (also referred to as BRPF2) which is a member of the BRD and plant homeodomain finger (BRPF) family of BRD-containing proteins (16,17). We specifically chose to focus on BRD1 because (i) it is already known to be essential in mice, suggesting it may be important in human cells; (ii) depletion of BRD1 leads to decreased proficiency in the repair of double strand DNA breaks by homologous recombination (HR), increased gamma irradiation sensitivity, and increased micronuclei formation, suggesting it likely has a role in DDR (18); (iii) BRD1 affinity purification-mass spectrometry analysis identified BRCA1, which functions in both RS and HR, as part of a larger BRD1 interactome (18); and (iv) it and other BRPF family members interact with the HBO1 histone acetyltransferase which functions in regulation of replication origins and has also been linked to DNA damage (17,19–22). Taken together, these results suggest that BRD1 may have a role in DDR or RS suppression, possibly together with HBO1 and/or BRCA1, and given the link to HBO1, potentially through replication origin regulation. This possibility is exciting since (i) replication origin activation is a known source of DNA damage at baseline (23), and (ii) dysregulation of replication origins is a known source of RS (3,4).

Replication origin regulation is a multi-step process. In G1 phase, origins are licensed when the pre-replication complex (pre-RC) consisting of origin recognition complex (ORC) proteins, mini-chromosome maintenance (MCM) proteins 2–7, and HBO1, among other factors, assembles on chromatin (20,24,25). At the G1-S transition, origin firing occurs when the pre-RC is phosphorylated by the CDC7 and/or possibly CDK1 kinase followed by cyclin E-CDK2 (26,27), and additional proteins which form the pre-initiation complex (pre-IC) are loaded at the origins, ultimately resulting in an active bidirectional replisome (24,25). Upregulated replication origin firing can cause or exacerbate RS by (i) depleting nucleotide pools required for fork progression, and (ii) allowing replication activation even in the setting of RS or DNA damage (3–5,28). Given the links between (i) BRD1 and DNA damage, (ii) BRD1 and HBO1, and (iii) replication origins and RS, we hypothesized that BRD1 may play a role in RS suppression or the RS response linked to replication origin regulation which is distinct from the BET family and other BRPF family members and may be therapeutically targetable in HGSC (17,18,22). We utilized functional, immunofluorescence, and sequencing assays in a panel of HGSC precursor and *BRCA1* mutant and wildtype ovarian cancer cell lines to test this hypothesis and also to test for links between BRD1 and BRCA1 in suppressing or responding to RS given the role of BRCA1 in protecting stalled replication forks (4,7).

Here, we show that BRD1 forms a RS suppressing complex with HBO1, BRCA1, and the BRCA1 stoichiometric binding partner BARD1, ORigin FIring Under Stress (ORFIUS), which regulates replication origins both at baseline and during RS. We show that the ORFIUS complex promotes eventual replication origin firing through BRD1 and HBO1 supported localization of the core replication origin licensing protein ORC2 at nuclear foci in a BRCA1 regulated manner. Upon BRCA1 mutation or depletion, basal origin firing and nuclei with BRD1, HBO1, and ORC2 foci increase; whereas, upon BRD1 or HBO1 depletion, basal origin firing and nuclei with ORC2 foci decrease. In normal or non-HGSC ovarian cancer cells, the ORFIUS complex disengages from origins and stops promoting localization of ORC2 to nuclear foci after DNA damage and/or RS. In *BRCA1* mutant and sporadic HGSC cells, the ORFIUS complex is dysregulated, present in excess in nuclear foci at baseline, and remains associated with replication origins promoting ORC2 localization in nuclear foci, even in the setting of DNA damage and/or RS. Reconstitution of BRCA1 expression in *BRCA1* mutant cells rescues this dysregulation. These findings suggest that ORFIUS complex dysfunction may represent a novel RS target in HGSC.

Materials and methods

For additional and more detailed Materials and methods, see Supplementary Materials and methods.

Tissue culture

Cell lines were purchased from American Type Culture Collection and validated by STR profiling in the Center for Patient-Derived Models at Dana-Farber Cancer Institute. Cell lines were utilized at low passage number and tested negative for mycoplasma by PCR. FT194 and FT237 cells were grown in

Dulbecco's Modified Eagle Medium (DMEM)/Nutrient Mixture F-12 (1:1) (Gibco Cat. #11320-033), 10% FBS (Sigma Cat. #F2442), and 1% penicillin streptomycin (P/S). OVCAR8, SKOV3, CaOV3, and CaOV4 cells were grown in Roswell Park Memorial Institute (RPMI) 1640 (Gibco Cat. #11875-093), 10% FBS, and 1% P/S. OVCAR3 cells were grown in RPMI 1640, 20% FBS, 0.01 mg/ml bovine insulin, and 1% P/S. UWB1.289 parent and UWB1.289 BRCA1 reconstituted cells were grown in 1:1 ATCC formulation RPMI 1640 (Gibco Cat. #A1049101)/Mammary Epithelial Cell Growth medium (MEGM) without amphotericin B (Lonza Cat. #CC-3150), 3% FBS, and 1% P/S. The reconstituted line was also grown in the presence of 200 μg/ml G-418 (Gibco Geneticin Cat. #10131-035). 293T cells were grown in DMEM (Gibco Cat. #11965-092), 10% FBS, and 1% P/S.

Oligonucleotide (oligo), short interfering RNA (siRNA), and short hairpin RNA (shRNA) sequences

Sequences for all oligos, siRNAs, and shRNAs are provided in Supplementary Materials and methods in either a list format or in Supplementary Tables S1, S2, or S3.

Immunofluorescence staining using methanol/acetic acid fixation

For transfection experiments, cells were transfected and plated on coverslips (Electron Microscopy Sciences Cat. #72228-01) and then either (i) fixed and stained, or (ii) treated with DMSO or 1μM Olaparib (MedChemExpress Cat. #HY-10162) and fixed at the appropriate timepoints. For non-transfected cells, the cells were plated on coverslips the night before, and then either (i) fixed and stained the next day or the following day, or (ii) treated with either (a) DMSO or 1μM Olaparib for 24 h or (b) DMSO, 1 μM AZD6738 (MedChemExpress Cat. # HY-19323), 1 μM XL-413 (MedChemExpress Cat. #HY-15260), or 1 μM Olaparib for 2–24 h, and then fixed and stained. On the day of staining, a 3:1 mixture of methanol:glacial acetic acid was prepared and chilled on ice for 20 min prior to use (Fisher Cat. #A412-4 and A38-500). The media was aspirated from the cells and the methanol/acetic acid solution was added for 15 minutes at 4°C. The cells were washed twice with PBS. Cells were then blocked for 30 min at 37°C in 1 mg/ml BSA, 5% normal goat serum, 1% Triton X-100, and PBS. The coverslips were then placed directly in primary antibody mixed with 1 mg/ml BSA, 5% normal goat serum, 1% Triton X-100, and PBS for 45 min at 37°C. The coverslips were washed twice in PBS and then incubated with secondary antibody mixed in 1mg/ml BSA, 5% normal goat serum, 1% Triton X-100, and PBS for 30 min at 37°C. The coverslips were washed twice in PBS and then mounted in mounting medium with DAPI (Vector Labs Cat. #H-2000) and sealed on a slide. Primary antibodies included BRD1 (Abcam Cat. #181060), HBO1 (Cell Signaling Technology Cat. #58418), HBO1 (Santa Cruz Biotechnology Cat. #sc-398346), ORC2 (Cell Signaling Technology Cat. #4736), and γH2AX (Millipore Sigma Cat. #05-636). Secondary antibodies included 488 anti-rabbit (Abcam Cat. #150077), 594 anti-mouse (Abcam Cat. #150116), and 555 anti-rat (Cell Signaling Technology Cat. #4417). For foci analysis, the percentage of nuclei with greater than or equal to three individual or co-localizing foci was quantified from at least 100 nuclei for each cell line or treatment in each individual experiment, and the average percentage of nuclei with greater than or equal to three foci is depicted in bar graphs in each figure as described in figure legends.

Immunofluorescence images

All immunofluorescence stained cells were photographed on a Zeiss Axio Imager M2 microscope with a Zeiss Axiocam 705 Mono Camera. Images were taken at 63× and 100×. For representative images, representative nuclei were cropped from a 63× or 100× image in Adobe Photoshop to demonstrate representative foci (Supplementary Figures S1E and S1F). If brightness and contrast were adjusted, they were adjusted in PowerPoint with the same manipulation performed on every image in a panel. All images for every experiment are available upon request. For the γH2AX exposures only in Figures 1G–I and 2E–G, the exposure time was lower for UWB1.289 parent and reconstituted cells versus OVCAR8 because of the high γH2AX signal in UWB1.289 cells. Thus, the UWB1.289 parent and reconstituted γH2AX foci counts in these figures can all be compared to each other, but the OVCAR8 data was taken at a higher exposure. The exposures utilized individually for BRD1, HBO1, and ORC2 were held constant across all cell lines and all panels in every figure throughout the manuscript including the above panels.

DNA fiber assay

OVCAR8 or FT194 cells were plated on day zero, transfected on days one and two, split one to two on day three, and then on day four (72 h post the first transfection), they were labelled for DNA fiber analysis. UWB1.289 parent and reconstituted cells were plated on day zero and labelled for DNA fiber analysis the following day. Cells were first pulsed with 0.2 mM CldU (5-chloro-2′-deoxyuridine) (Sigma Cat. #C6891) for 30 min at 37°C. Cells were then washed twice with pre-warmed PBS. Cells were then pulsed with 0.25 mM IdU (5-iodo-2′-deoxyuridine) (Sigma Cat. #I7125) for 30 min at 37°C. Cells were washed with pre-warmed PBS twice. Cells were combed and stained as described previously (29). For a detailed staining protocol, please see Supplementary Materials and methods. The fibers were photographed at 40× and scored as described below. All fiber scoring was performed by two individuals counting independently from each other, with the resulting percentages within two percent of each other's counts.

Each distinct fiber was scored based on its replication structure identified as the following, with the first pulse CldU stained green and the second pulse IdU stained red: (i) ongoing fork: adjacent green and red signal; (ii) bidirectional fork consisting of origin fired during the first pulse labeling: connecting red-green-red signal; (iii) new origin fired during the second pulse labeling: red signal only; (iv) termination: connecting green-red-green signal; (v) stalled fork: green signal only (30). At least 200 fibers were scored for each treatment, and each experiment was repeated independently three separate times. The percentage of new origins fired was calculated as follows, with origins being the sum of those origins fired during the first (CldU green) and the second (IdU red) pulse labeling (2 + 3 above) (26):

% origins = origins/(origins + ongoing forks)

Chromatin immunoprecipitation sequencing (ChIP-seq)

Five 80% confluent plates of UWB1.289 parent cells were grown per antibody and media changed the day before the

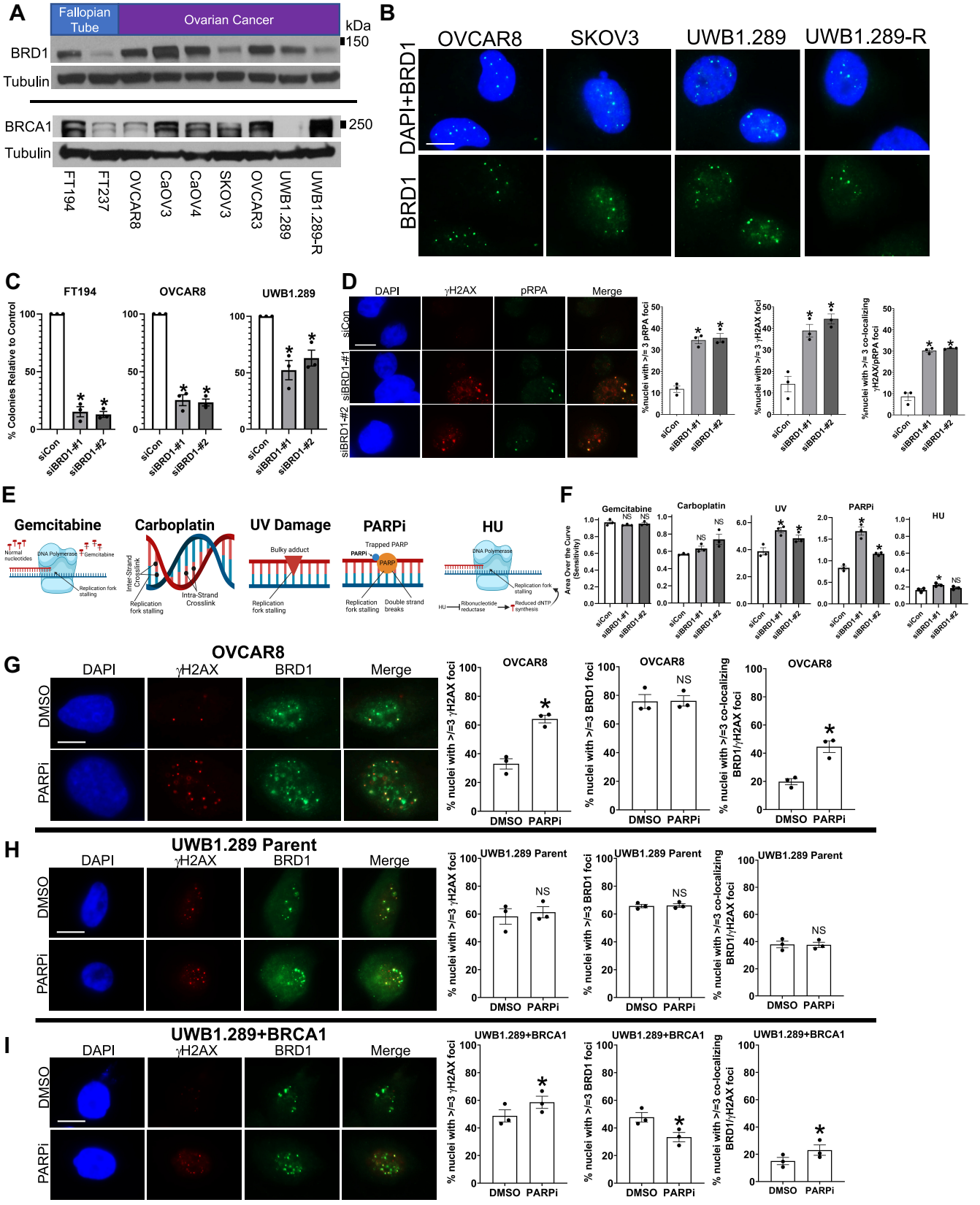

Figure 1. BRD1 suppresses replication stress at structures susceptible to PARP inhibitor-induced DNA damage and/or replication stress. (**A**) Western blot analyses for BRD1 (top) and BRCA1 (bottom) were performed on lysates from a group of fallopian tube secretory epithelium and ovarian cancer cell lines (UWB1.289 reconstituted with full length BRCA1 = UWB1.289-R). The cell line type is denoted by color code on the top of the blot. Tubulin is shown as a loading control for each western. Please note, a single gel was run for the BRD1 and HBO1 western blots in Figures 1A (top) and 2A to allow for comparison of BRD1 and HBO1 from the same lysate at the same time. The membrane from the gel was first stained for BRD1, stripped and

experiment to basal media containing DMSO at 1:10,000, harvested 24 h later, chromatin prepared, and immunoprecipitation carried out using the Cell Signaling SimpleChIP Enzymatic Chromatin IP Kit following the manufacturer's protocol (Catalog #9003). Chromatin was prepared only once, and then that chromatin prep was divided into two aliquots, #1 and #2, to allow for later replicates. Two individual BRD1 or HBO1 IPs were performed for each of the #1 and #2 aliquots, and a separate input was saved from each of the #1 and #2 aliquots. Thus, there is a #1 and a #2 replicate for each IP antibody and each input. 5 μg of chromatin were used per IP. Antibodies for ChIP included HBO1 (Cell Signaling Cat. #58418) and BRD1 (Abcam Cat. #ab181060). Active Motif's spike-in controls were used according to the manufacturer's protocol (Cat. #61686 and 53083). ChIP-seq libraries were prepared using IDT xGen DNA library prep reagents on a Beckman Coulter Biomek i7 liquid handling platform from approximately 1ng of DNA with 14 cycles of PCR amplification according to manufacturer's protocol. Finished sequencing libraries were quantified by Qubit fluorometer and Agilent TapeStation 2200. Library pooling and indexing was evaluated with shallow sequencing on an Illumina MiSeq. Subsequently, libraries were sequenced on an Illumina NovaSeq6000 targeting 40 million 150 bp read pairs by the Molecular Biology Core facilities at Dana-Farber Cancer Institute. Please see the Supplementary Materials and methods for details on ChIP-seq analysis.

Statistics

All experiments were performed in duplicate or in triplicate. *P*-values were generated using a standard paired two-tailed *t*-test for single comparisons and a one-way ANOVA or a two-way ANOVA with post-hoc multiple comparisons test as indicated in respective figure legends. All analyses were performed in GraphPad Prism.

Results

BRD1 is expressed and promotes survival in ovarian cancer precursor and tumor cell lines

We first asked whether BRD1 is widely expressed in ovarian cancer and if the expression is altered in *BRCA1* mutant cells, since others have observed a potential interaction between BRD1 and BRCA1 and since BRCA1 has a role in protecting stalled replication forks (4,7,18). We tested the ovarian cancer precursor fallopian tube secretory epithelial (FTSEC) cell lines FT194 and FT237, the non-HGSC ovarian cancer cell line SKOV3, the sporadic HGSC cell lines OVCAR8, OVCAR3, CaOV3, and CaOV4, and the *BRCA1* mutant HGSC cell line UWB1.289 along with its full length BRCA1 reconstituted clone (Figure 1A) (31–36). Using an siRNA validated antibody (Supplementary Figure S1A), we were able to detect varying levels of BRD1 protein expression in all cell lines (Figure 1A). Full length BRCA1 (p220) was detected in all lines except for the parental UWB1.289 line (Figure 1A, Supplementary Figure S1B), which harbors a nonsense mutation in BRCA1 exon 11 preventing it from expressing p220 but allowing it to retain expression of the minimally functional Δ11 isoform (Supplementary Figures S1C, S1D) (32,37). BRD1 protein levels were reduced in the full length BRCA1 reconstituted UWB1.289 cells compared to the parent line (Figure 1A). These results indicate that BRD1 is widely expressed in ovarian cancer and suggest possible regulation of BRD1 by BRCA1.

We next addressed localization of BRD1 in HGSC cells. Immunofluorescent staining revealed that BRD1 forms distinct nuclear foci across different ovarian cancer subtypes and

←

re-stained for Tubulin, and finally stripped and re-stained for HBO1. The BRD1 blot and Tubulin blot from that single gel are shown on the top of Figure 1A. The HBO1 blot along with the same Tubulin blot from that gel are shown in Figure 2A for comparison. The BRCA1 western blot in Figure 1A (bottom) is from a separate gel with its own respective loading control. (**B**) OVCAR8, SKOV3, UWB1.289 parent, and UWB1.289 reconstituted with full length BRCA1 (UWB1.289-R) cells were immunofluorescently stained for BRD1. DAPI was used as a nuclear stain. Representative nuclei are shown with BRD1 and DAPI overlaid in the top panel and BRD1 alone in the bottom panel. Scale bar = 10 μm. (**C**) FT194, OVCAR8, and UWB1.289 cell lines were transfected with either a control (siCon) or two different BRD1-specific siRNAs (siBRD1-#1 and siBRD1-#2) and plated for colony formation. Results are depicted as bar graphs showing the average percentage of colonies relative to the control for three individual experiments with error bars representing standard error of the mean. $*P < 0.05$ compared to the control by a standard *t*-test. (**D**) Immunofluorescence staining for γH2AX and phosphorylated RPA (pRPA) was performed on OVCAR8 cells transfected with a control siRNA (siCon) or two BRD1-specific siRNAs (siBRD1-#1 and siBRD1-#2) 48 h after the first transfection. Representative images of nuclei for each stain for each treatment are shown on the left. Scale bar = 10 μm. Bar graphs representing the average percentage of nuclei with greater than or equal to three pRPA, γH2AX, or co-localizing pRPA/γH2AX foci for each treatment from three independent experiments are shown on the right with error bars representing standard error of the mean. $*P < 0.05$ compared to the control by a standard *t*-test. (**E**) Cartoon illustrating the mechanism of action of different replication stress inducing agents which either (i) stall forks directly, like gemcitabine or hydroxyurea (HU), or (ii) generate obstacles in the DNA which cause replication fork stalling, including crosslinks caused by carboplatin, bulky adducts caused by UV, and trapped PARP caused by PARP inhibitors (PARPi). **(F)** OVCAR8 cells were transfected with a control siRNA (siCon) and two BRD1 specific siRNAs (siBRD1-#1 and siBRD1-#2). For gemcitabine, carboplatin, HU, and the PARPi Olaparib, cells were plated and treated with dose curves of the respective agents or media with no drug for a small subset of wells. For the wells that received no drug, CellTiter-Glo was immediately added and the plate was read to generate a day one read for later growth rate correction. For the dose curve treated cells, survival was assessed five days later via CellTiter-Glo. Growth rate corrected dose curves were generated by mathematically comparing the day five reads to the day one read of untreated cells to correct for any growth rate differences. The sensitivities shown here were generated by calculating the area over the growth rate corrected dose curve for each agent shown (greater area = greater sensitivity to the agent). For UV treatment, transfected cells were plated at a suitable density for colony formation on day one and treated with a dose curve of UV irradiation. Seven days later the colonies were stained and counted, and survival curves were generated. The sensitivity was calculated as the area over the survival curve. The bar graphs represent the average from three separate experiments with error bars representing standard error of the mean. *P*-values were generated using a standard *t*-test, and $*P < 0.05$ compared to the control. NS = not significant compared to the control. Please also see Supplementary Figure S2C for representative survival or dose curves. (**G–I**) OVCAR8, UWB1.289 parent, or BRCA1 reconstituted UWB1.289 (UWB1.289 + BRCA1) cells were treated with vehicle (DMSO) or 1 μM of the PARP inhibitor (PARPi) Olaparib for 24 h and then immunofluorescently stained for γH2AX and BRD1. In each panel, representative images of nuclei with foci are shown on the left. Scale bars = 10μm. Bar graphs representing the average percentage of nuclei with greater than or equal to three γH2AX, BRD1, or co-localizing γH2AX/BRD1 foci from three independent experiments are shown on the right. Error bars represent standard error of the mean. *P*-values were calculated using a standard *t*-test, and $*P < 0.05$ compared to DMSO. NS = not significant compared to DMSO.

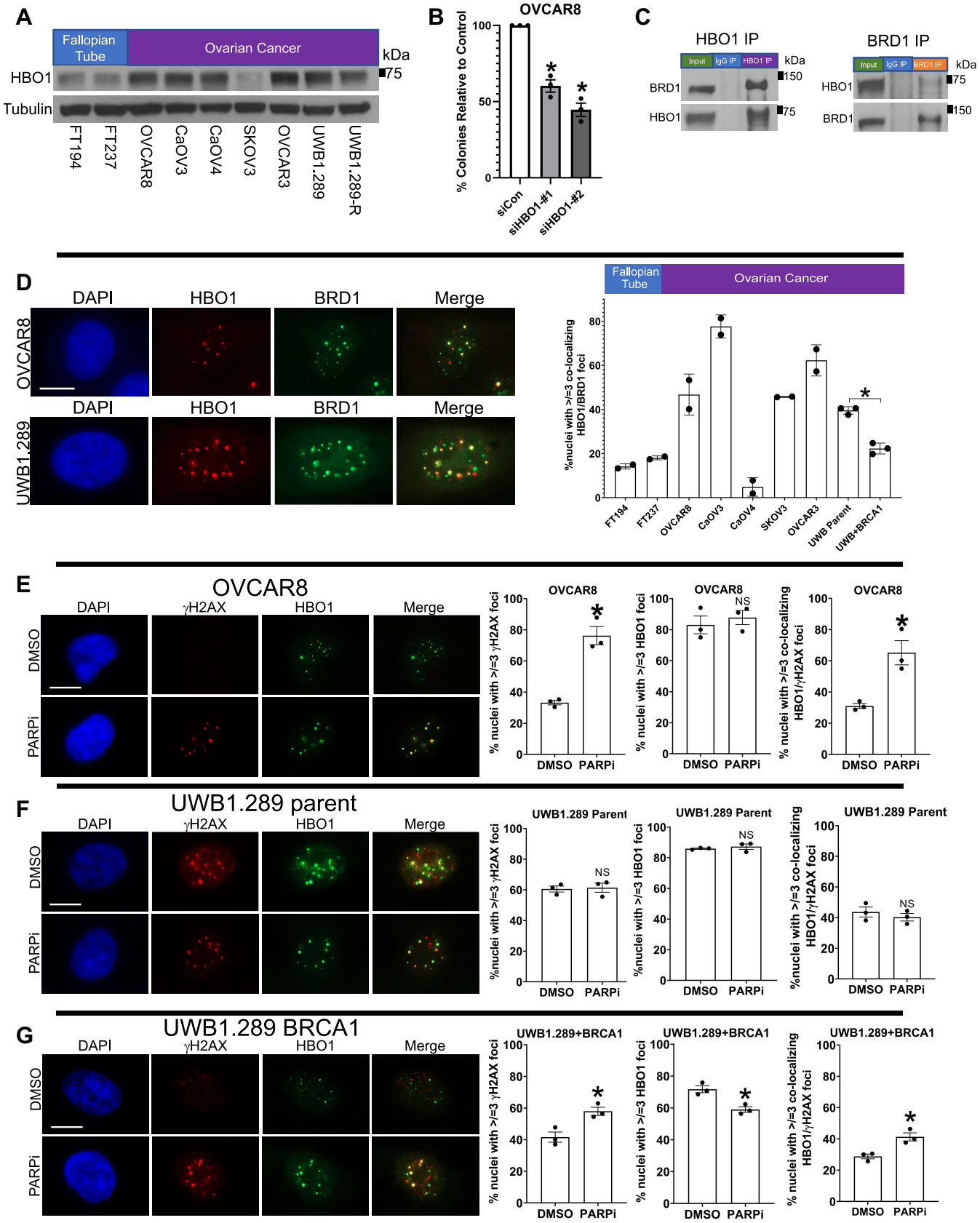

Figure 2. BRD1 forms a complex with HBO1 which may help suppress replication stress in HGSC cells. (**A**) Western blot analysis for HBO1 was performed on lysates from a group of ovarian cancer precursor fallopian tube secretory epithelium cell lines and ovarian cancer cell lines (UWB1.289 parent reconstituted with full length BRCA1 = UWB1.289-R). The cell line type is denoted by color code on the top of the blot. Tubulin is shown as a loading control. Please note, a single gel was run for the BRD1 and HBO1 western blots in Figures 1A (top) and 2A to allow for comparison of BRD1 and

genetic backgrounds (Figure 1B, Supplementary Figures S1E, S1F).

Next we assessed whether BRD1 is important for ovarian cancer precursor and tumor cell survival. BRD1 depletion caused reduced colony formation compared to a control in FT194, OVCAR8, and UWB1.289 cells (Figure 1C). These results suggest that BRD1 promotes survival in ovarian cancer precursor and tumor cells.

BRD1 helps suppress RS linked to bulky adducts and PARP inhibitors

Since others have noted that inhibition of BRD4 and other BET family members leads to RS and/or DNA damage, our next question was whether loss of BRD1 also does (12–15,18). We stained OVCAR8 cells treated with control or BRD1 siRNAs for γH2AX which can be a marker of DNA damage or RS, as well as Replication Protein A phosphorylated on serine 33 (pRPA) which is a marker of single stranded DNA at stalled replication forks indicative of RS (3). After depletion of BRD1 in OVCAR8 cells, we noted an increased percentage of nuclei with γH2AX, pRPA, and co-localizing γH2AX and pRPA foci (Figure 1D). The increase in the percentage of nuclei with pRPA foci alone indicates a role for BRD1 in suppressing RS, and the increase in the percentage of nuclei with γH2AX and co-localizing foci may indicate a role in suppressing DNA damage at sites of RS. This suggests that BRD1 has a distinct baseline role in RS suppression among BRPF family members, as depletion of the related BRPF family protein BRPF3 does not lead to changes in the percentage of nuclei with γH2AX, pRPA, or co-localizing γH2AX/pRPA foci (Supplementary Figures S2A, S2B) (22).

Our next question was what type of RS BRD1 might suppress. We treated HGSC cells with multiple BRD1-specific siRNAs versus a control and tested for sensitivity to agents which stall replication forks directly or generate obstacles in the DNA which cause fork stalling. Increased sensitivity after BRD1 depletion would indicate a role for BRD1 in protection from the type of RS induced by the specific agent. We tested the nucleoside analog gemcitabine which incorporates into nascently replicating DNA strands and prevents additional nucleosides from incorporating thereby causing fork stalling, carboplatin which induces crosslinks which can stall forks, the PARPi Olaparib which causes PARP trapping and subsequent fork stalling, ultraviolet radiation (UV) which induces bulky adducts which can stall forks, and hydroxyurea (HU) which leads to deoxyribonucleotide depletion and subsequent fork stalling (Figure 1E) (4). BRD1 depletion led to increased sensitivity to both PARPis and UV compared to control treated cells (Figure 1F, Supplementary Figure S2C). BRD1 depletion did not lead to increased sensitivity to gemcitabine, led to a minor increase in sensitivity to HU with only one siRNA, and only caused a minor and not significant increase in sensitivity to carboplatin (Figure 1F, Supplementary Figure S2C). These results support that BRD1 may participate in protection from bulky adduct- and PARPi-induced RS and/or DNA damage, and our next question was how it does so. Given their heavy clinical use in HGSC, we utilized PARPis to study the role of BRD1 in RS in the remainder of our experiments (8).

BRD1 associates with nuclear structures in which PARPis induce DNA damage and/or RS

Multiple groups have shown that the BRD-containing protein BRD4 regulates DDR or RS suppression at the transcriptional level (12–14), while others have shown direct roles for BET or other BRPF BRD-containing proteins in DNA damage and RS suppression (15,18,22,38). Our next question was whether BRD1 directly or transcriptionally participates in protection from PARPi-associated RS and/or DNA damage.

We had already shown that BRD1 forms distinct nuclear foci at baseline (Figure 1B). Thus, to test for a direct role for BRD1 in suppressing PARPi-induced RS or DNA damage we treated OVCAR8 cells and the isogenic pair of UWB1.289 parent and the full length BRCA1 reconstituted clone with vehicle or a PARPi and quantified the percentage of nuclei with individual and co-localizing BRD1 and γH2AX foci. In OVCAR8 cells, we observed an increased percentage of nuclei with co-localization of BRD1 with γH2AX post-PARPi (Figure 1G). The co-localization was driven by a large increase in the percentage of nuclei with γH2AX foci and with no change in the percentage of nuclei with BRD1 foci after PARPi treatment (Figure 1G). In the parent UWB1.289 line post-PARPi there was no change in the percentage of nuclei with BRD1/γH2AX foci co-localization, a small but not significant increase in the percentage of nuclei with γH2AX foci, and no change in the percentage of nuclei with BRD1 foci versus vehicle (Figure 1H). In the BRCA1 reconstituted UWB1.289 line, there was a

←

HBO1 from the same lysate at the same time. The membrane from the gel was first stained for BRD1, stripped and re-stained for Tubulin, and finally stripped and re-stained for HBO1. The BRD1 blot and Tubulin blot from that single gel are shown on the top of Figure 1A. The HBO1 blot along with the same Tubulin blot from that gel are shown here in Figure 2A for comparison. The BRCA1 western blot in Figure 1A (bottom) is from a separate gel with its own respective loading control. (**B**) OVCAR8 cells were transfected with either a control siRNA (siCon) or two HBO1-specific siRNAs (siHBO1-#1 and siHBO1-#2) and plated for colony formation. A bar graph representing the average percentage of colonies relative to the control for three individual experiments is shown with error bars representing standard error of the mean. $*P < 0.05$ compared to the control by a standard *t*-test. (**C**) Immunoprecipitation experiments were performed in OVCAR8 cells. On the left, lysates from untreated OVCAR8 cells were immunoprecipitated with IgG control versus an HBO1 antibody and blotted with BRD1 antibody on the top or a different HBO1 antibody on the bottom. On the right, lysates from untreated OVCAR8 cells were immunoprecipitated with IgG control versus a BRD1 antibody and blotted with HBO1 antibody on the top and BRD1 antibody on the bottom. In each case, western type, input, or IP type is indicated on top of the blot. (**D**) Untreated fallopian tube and ovarian cancer cell lines (UWB1.289 parent (UWB parent) reconstituted with full length BRCA1 = UWB + BRCA1) were immunofluorescently stained for BRD1 and HBO1. Representative images of nuclei with foci from OVCAR8 (top) and UWB1.289 parent (bottom) are shown in the left panel. Scale bars = 10 μm. A bar graph representing the average percentage of nuclei with greater than or equal to three co-localizing BRD1/HBO1 foci from two individual experiments for most lines and three individual experiments for UWB parent and UWB + BRCA1 is shown on the right. Cell type is indicated on top of the bar graph. Error bars represent standard deviation. $*P < 0.05$ compared to the UWB parent line by a standard *t*-test. (**E–G**) OVCAR8, UWB1.289, or BRCA1 reconstituted UWB1.289 (UWB1.289 + BRCA1) cells were treated with vehicle (DMSO) or 1 μM of the PARP inhibitor (PARPi) Olaparib for 24 h and then immunofluorescently stained for γH2AX and HBO1. In each panel, representative images of nuclei with foci are shown on the left. Scale bars = 10 μm. A bar graph representing the average percentage of nuclei with greater than or equal to three γH2AX, HBO1, or co-localizing γH2AX/HBO1 foci for each treatment from three separate experiments is shown on the right. Error bars represent standard error of the mean. *P*-values were calculated using a standard *t*-test, and $*P < 0.05$ compared to DMSO. NS = not significant compared to DMSO.

small but significant increase in the percentage of nuclei with co-localizing BRD1/γH2AX foci post-PARPi (Figure 1I). This was driven by a small but significant increase in the percentage of nuclei with γH2AX foci and a small but significant decrease in the percentage of nuclei with BRD1 foci post-PARPi (Figure 1I). Additionally, we observed a higher percentage of nuclei with co-localization of BRD1 with γH2AX at baseline in the parent UWB1.289 line than the reconstituted line (Figures 1G–I).

The increased percentage of nuclei with co-localization of BRD1 and DNA damage foci in OVCAR8 and reconstituted UWB1.289 cells post-PARPi suggests a direct and not transcription mediated role for BRD1 in RS or resulting DNA damage, and the fact that it is driven by a post-PARPi increase in the percentage of nuclei with γH2AX foci suggests that BRD1 is located on replication-linked structures at which PARPis induce DNA damage. The increased DNA damage in BRD1 foci at baseline in the UWB1.289 parent line compared to the reconstituted clone suggests that BRCA1 prevents DNA damage or RS in BRD1 structures at baseline. The fact that the percentage of nuclei with BRD1 foci start to decrease after PARPi treatment in the reconstituted but not the parent UWB1.289 and OVCAR8 lines suggests that normally BRCA1 may block BRD1 localization at replication associated structures in the setting of PARPi-induced RS to suppress RS and/or DNA damage, but in sporadic and *BRCA1* mutant HGSC cells this localization is dysregulated.

BRD1 interacts with HBO1 in HGSC cells

Our next question was what replication or RS suppression function BRD1 participates in. We assessed what proteins BRD1 interacts with to search for possible functions based on the known functions of interacting partners. A major interacting partner of BRD1 is the histone acetyltransferase HBO1 (also referred to as KAT7) which modifies histones H3 and H4 (17,39). HBO1 has known functions in replication origin licensing and firing with multiple different binding partners (20,22,25). It interacts with ORC1, MCM2, and CDT1, and is part of the pre-RC which promotes replication origin licensing (20,40–42). It has been linked to DNA damage through its role in the nucleotide excision repair pathway (21). HBO1 expression is frequently upregulated in many cancer types (43–45). These HBO1 factors make it a logical BRD1-interacting partner to test as a possible member of a BRD1 replication or RS-suppression complex.

We first verified HBO1 protein expression in our panel of fallopian tube and ovarian cancer cell lines using an siRNA validated HBO1 antibody, and found it to be expressed in all cell lines, again with a very slight decrease in the *BRCA1* reconstituted UWB1.289 cells versus their parent line (Figure 2A, Supplementary Figure S2D). This suggests that like BRD1, HBO1 is widely expressed in ovarian cancer and may be controlled by BRCA1.

We next assessed whether HBO1 is important for ovarian cancer cell survival. Others have demonstrated that HBO1 is not essential in non-HGSC cell lines lacking background DDR defects (46). Since many HGSC cells have DDR deficiency or upregulated RS, we hypothesized that the HBO1 function in DDR and/or replication may be upregulated or important for survival of these cells. Indeed, in OVCAR8 cells, HBO1 depletion causes reduced colony formation compared to control siRNA treated cells (Figure 2B) suggesting that HBO1 promotes survival in at least some HGSCs.

Our next question was whether BRD1 and HBO1 interact in ovarian cancer cells since they are known to physically interact in other cell types (17,39). We performed co-immunoprecipitation of HBO1 by BRD1 and BRD1 by HBO1 and found that the proteins are able to endogenously interact via either precipitating partner in both OVCAR8 (Figure 2C) and UWB1.289 cells (Supplementary Figure S2E). This suggests that the proteins maintain their interaction across HGSC genotypes.

Our next question was whether HBO1 forms nuclear foci, and if so, whether BRD1 and HBO1 co-localize and how often in ovarian cancer precursor and tumor cell lines. We were able to detect HBO1 nuclear foci in OVCAR8 cells with multiple antibodies (Supplementary Figure S2F). Immunofluorescent co-staining for BRD1 and HBO1 showed large percentages of nuclei with co-localization in most ovarian cancer cell lines but markedly less in the precursor fallopian tube lines FT194 and FT237 (Figure 2D). The CaOV4 HGSC line showed limited nuclei with HBO1/BRD1 co-localization despite protein expression suggesting a potential alteration in localization of these proteins to nuclear foci in this cell line (Figures 1A, 2A and D). Finally, the *BRCA1* reconstituted UWB1.289 cells showed a significantly lower percentage of nuclei with co-localizing foci than the parent UWB1.289 line (Figure 2D). These results suggest that co-localization of BRD1 and HBO1 is upregulated in both HGSC and non-HGSC ovarian cancer cells compared to HGSC precursor fallopian tube cells and support that BRCA1 regulates the BRD1–HBO1 complex.

Knowing that BRD1 and HBO1 co-localize, that PARPis induce DNA damage and/or RS in BRD1 nuclear foci, and that HBO1 has a DNA damage and replication function, our next question was whether PARPis also induce DNA damage and/or RS in HBO1 nuclear foci. We treated OVCAR8 cells and the isogenic pair of UWB1.289 and its reconstituted clone with vehicle versus PARPi and stained for γH2AX and HBO1. We found that in OVCAR8 and BRCA1 reconstituted UWB1.289 cells, there is an increased percentage of nuclei with co-localization of HBO1 with γH2AX after PARPi, whereas in the UWB1.289 parent line the percentage of nuclei with co-localization is unchanged after PARPi, as with BRD1 (Figures 2E, 2F, 2G). Also, as with BRD1, there is a lower percentage of nuclei with co-localizing HBO1/γH2AX foci at baseline in the BRCA1 reconstituted UWB1.289 line compared to the parent line (Figures 2F and G). The increasing percentage of nuclei with co-localization in OVCAR8 and BRCA1 reconstituted UWB1.289 cells is driven by an increase in the percentage of nuclei with γH2AX foci, with no change in the percentage of nuclei with HBO1 foci post-PARPi in OVCAR8 cells and a decrease in the percentage of nuclei with HBO1 foci post-PARPi in reconstituted UWB1.289 cells (Figures 2E and G). There is no change in the percentage of nuclei with γH2AX or HBO1 foci after PARPi in the UWB1.289 parent line (Figure 2F). These data reveal that like BRD1, HBO1 is located at structures susceptible to PARPi-induced RS and/or DNA damage which require BRCA1 for repair. Additionally, they suggest that HBO1 localization at these structures is regulated by BRCA1, and that in both sporadic and *BRCA1* mutant HGSC cells HBO1 localization in nuclear foci may be dysregulated in the setting of PARPi-induced RS and/or DNA damage.

The BRD1–HBO1 complex helps promote replication origin firing in HGSC cells

Our next question was what the role of the BRD1–HBO1 complex is in DNA replication. We focused on a role for the BRD1–HBO1 complex in replication origin regulation given that HBO1 is already known to participate in both replication origin licensing and firing with different binding partners (22,42).

To determine if BRD1 and HBO1 promote replication origin firing in HGSC cells, we utilized a DNA fiber assay in which we pulse cells sequentially with two nucleoside analogs to label nascently replicated DNA fibers, comb and stain the fibers, and then quantify the percentage of fibers representing newly fired replication origins amongst all the different replication fiber types (Figure 3A) (26,47). We quantified the percentage of newly fired replication origins in OVCAR8 cells after BRD1 or HBO1 depletion compared to a control at a post-depletion timepoint when we were certain there was no cell cycle arrest (Figures 3B and C, Supplementary Figures S3A, S3B). We found that there is decreased origin firing in the setting of HBO1 depletion as expected and also in the setting of BRD1 depletion (Figures 3B and C). This suggests that the BRD1-HBO1 protein complex participates in some aspect of replication origin regulation ultimately leading to origin firing in HGSC cells.

The BRD1–HBO1 protein complex physically localizes to ORC2 marked replication origins

Our next question was whether the BRD1–HBO1 complex regulates replication origins directly or indirectly. HBO1 is already known to physically associate with replication origins and members of the origin regulatory pre-RC (20,25,40–42). Given this and the tight physical association between BRD1 and HBO1 (Figures 2C and D, Supplementary Figure S2E), we hypothesized that at least some of the nuclear BRD1–HBO1 co-localizing foci we observe are at replication origins performing a direct regulatory role in HGSC cells.

To validate this, we tested for co-localization of BRD1 and HBO1 nuclear foci with the origin recognition complex protein ORC2, which is part of the pre-RC and is known to specifically bind to replication origin sites in the DNA (48). We found that ORC2 is widely expressed in our fallopian tube and ovarian cancer cell line panel and forms nuclear foci (Figure 3D, Supplementary Figures S3C, S3D). We detected varying percentages of nuclei with co-localization of BRD1 and HBO1 with ORC2 in our cell line panel (Figures 3E, 3F, 3G, 3H). CaOV4 cells formed less ORC2, BRD1, and HBO1 foci than other ovarian cancer cells, as previously shown (Figures 2D, 3F and H). Sporadic and *BRCA1* mutant HGSC cells demonstrated both increased percentages of nuclei with co-localizing BRD1/ORC2 and HBO1/ORC2 foci and ORC2 foci alone than FTSEC precursor controls and the non-HGSC ovarian cancer line SKOV3 (Figures 3F and H). Ovarian cancer cells demonstrated increased percentages of nuclei with HBO1 and BRD1 foci alone than FTSEC cells (Figures 3F and H). Additionally, the UWB1.289 parent line demonstrated both a significantly increased percentage of nuclei with both individual ORC2, BRD1, and HBO1 foci and co-localizing BRD1/ORC2 and HBO1/ORC2 foci compared to the BRCA1 reconstituted clone.

These results suggest that (i) ORC2 localization at nuclear foci is upregulated in sporadic and *BRCA1* mutant HGSC cells and is likely regulated by BRCA1, (ii) BRCA1 regulates the localization of BRD1 and HBO1 to replication origins potentially as part of a BRCA1–BRD1–HBO1 complex, and (iii) localization of BRD1 and HBO1 at origins is dysregulated in sporadic and *BRCA1* mutant HGSC. Our next question was, how do HBO1, BRD1, and BRCA1 regulate each other and possibly ORC2.

HBO1 helps maintain BRD1 protein levels and together they promote ORC2 localization in nuclear foci

To begin to assess BRD1/HBO1/BRCA1/ORC2 dynamics, we first addressed whether HBO1 recruits BRD1 to nuclear foci or vice versa. Upon BRD1 depletion, HBO1 still formed nuclear foci in OVCAR8 cells (Figure 4A). However, upon HBO1 depletion, less and smaller BRD1 foci were detectable in OVCAR8 cells (Figure 4B). Similarly, after HBO1 depletion, there was a reduced percentage of nuclei with BRD1/γH2AX co-localizing foci after PARPi treatment, but no change in the percentage of nuclei with HBO1/γH2AX co-localizing foci in the setting of BRD1 depletion after PARPi treatment (Figure 4C, Supplementary Figure S4A). This suggests that either HBO1 recruits BRD1 to nuclear foci at baseline or that HBO1 helps maintain BRD1 protein levels.

We tested if HBO1 or BRD1 depletion led to a reduction in protein levels of either binding partner and also in BRCA1 and ORC2 given the regulatory dynamics between these proteins. Upon depletion of BRD1 in OVCAR8 cells, HBO1 protein levels remain unchanged, whereas upon depletion of HBO1, BRD1 protein levels decrease (Figure 4D). BRCA1 and ORC2 protein levels remain unchanged after both BRD1 and HBO1 depletion compared to the control (Figure 4D). This suggests that HBO1 helps maintain BRD1 protein levels and that neither BRD1 or HBO1 helps maintain ORC2 or BRCA1 protein levels.

However, given the high percentage of nuclei with ORC2 foci alone or co-localizing ORC2/HBO1 and ORC2/BRD1 foci for most HGSC cells, our final question was whether HBO1 and/or BRD1 might regulate localization of ORC2 to nuclear foci (Figures 3F and H). To be certain that no observed phenotypes could be attributed to a cell cycle arrest, we assessed cell cycle profiles after BRD1 and HBO1 depletion and found no changes in cell cycle dynamics (Figure 4E). Upon depletion of BRD1, as expected there was no change in the percentage of nuclei with HBO1 foci, but there was a significant decrease in both the percentage of nuclei with ORC2 foci and co-localizing ORC2/HBO1 foci (Figure 4F). Upon depletion of HBO1, the percentage of nuclei with BRD1 foci was strongly reduced, and there was also a significant decrease in the percentage of nuclei with ORC2 foci and co-localizing ORC2/BRD1 foci (Figure 4G). In contrast, upon depletion of the related BRPF family member BRPF3, there was no change in the percentage of nuclei with individual ORC2, HBO1, or BRD1 foci or co-localizing ORC2/BRD1 or ORC2/HBO1 foci, nor were there any changes in BRD1, HBO1, ORC2, or BRCA1 protein levels (Supplementary Figures S4B, S4C, S4D, S4E, S4F). Taken together, these results suggest a unique role for BRD1 and HBO1 in promoting ORC2 localization to nuclear foci.

Given that ORC2 regulation is a novel role for BRD1 and HBO1, we sought to further validate this function (20,22,42). Therefore, we generated OVCAR8 cells stably expressing

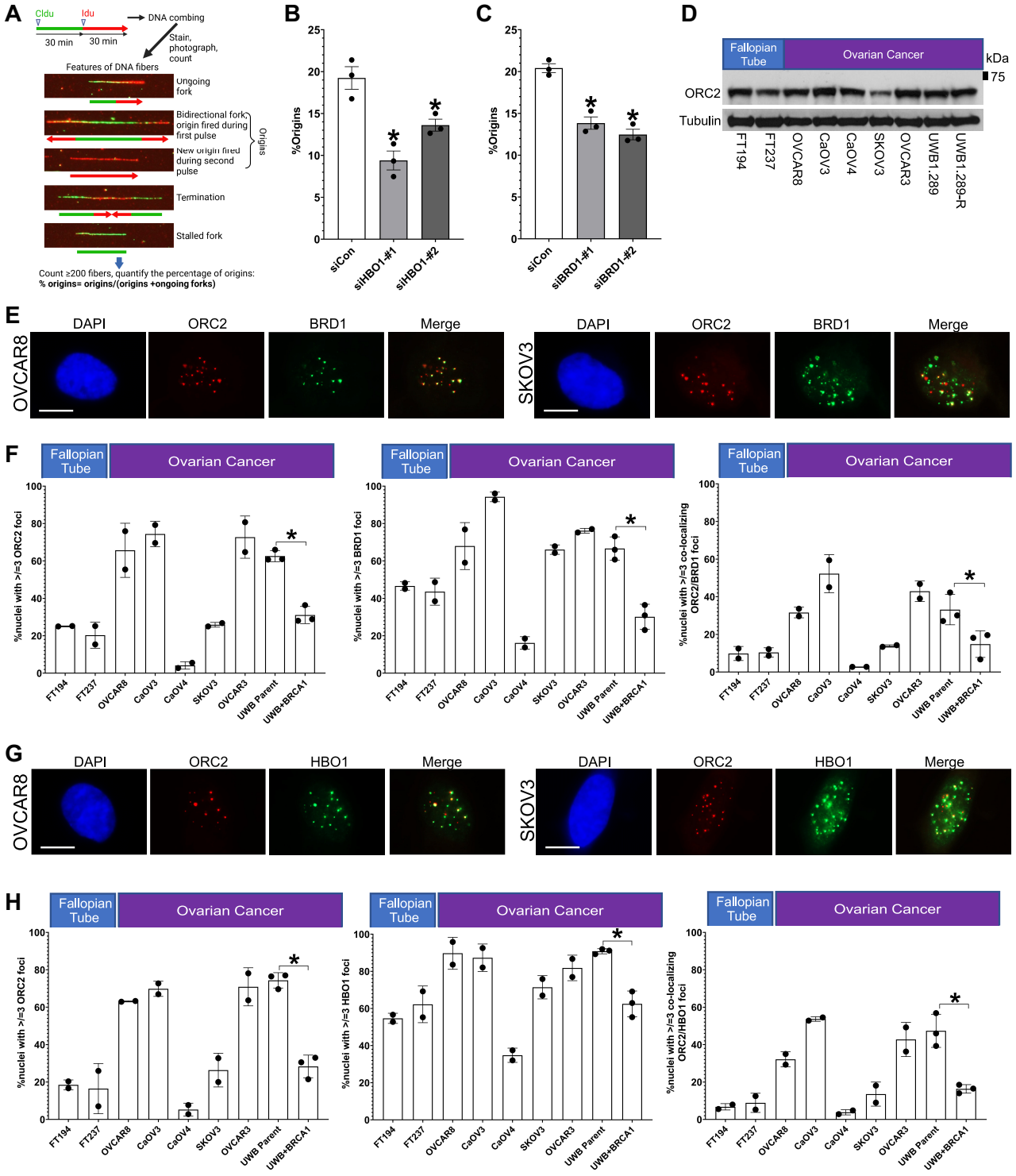

Figure 3. The BRD1–HBO1 complex functions in replication origin control. (**A**) Schematic of DNA fiber assay labeling, fiber scoring, and %origin calculation. (**B** and **C**) OVCAR8 cells were transfected with a control siRNA (siCon) or in (B) two HBO1 specific siRNAs (siHBO1-#1 and siHBO1-#2) or in (C) two BRD1 specific siRNAs (siBRD1-#1 and siBRD1-#2). 72 h after the first transfection, the cells were labeled for DNA fiber analysis and fibers stained. Fibers were scored to assess the percentage of firing replication origins. The bar graph represents the average percentage of firing origins from three independent experiments for each siRNA. Error bars represent standard error of the mean. $*P < 0.05$ compared to the control by a standard *t*-test. (**D**) Western blot analysis for ORC2 was performed on lysates from fallopian tube and ovarian cancer cell lines (UWB1.289 reconstituted with full length BRCA1 = UWB1.289-R). The cell line type is denoted by color code on the top of the blot. Tubulin is shown as a loading control. (**E–H**) Untreated fallopian tube and ovarian cancer cell lines (UWB1.289 parent (UWB parent) reconstituted with full length BRCA1 = UWB + BRCA1) were immunofluorescently stained for BRD1 and ORC2 in (E) and (F) or HBO1 and ORC2 in (G) and (H). Representative images of nuclei with foci from OVCAR8 (left) and SKOV3 (right) are shown in (E) and (G) for each staining pattern. Scale bars = 10 μm. Bar graphs representing the average percentage of nuclei with greater than or equal to three ORC2, BRD1, or co-localizing ORC2/BRD1 foci in (F) or ORC2, HBO1, or co-localizing ORC2/HBO1 foci in (H) from two individual experiments for most lines and three individual experiments for UWB parent and UWB + BRCA1 are shown. Cell type is indicated on top of the bar graph. Error bars represent standard deviation. $*P < 0.05$ compared to the UWB parent line by a standard *t*-test.

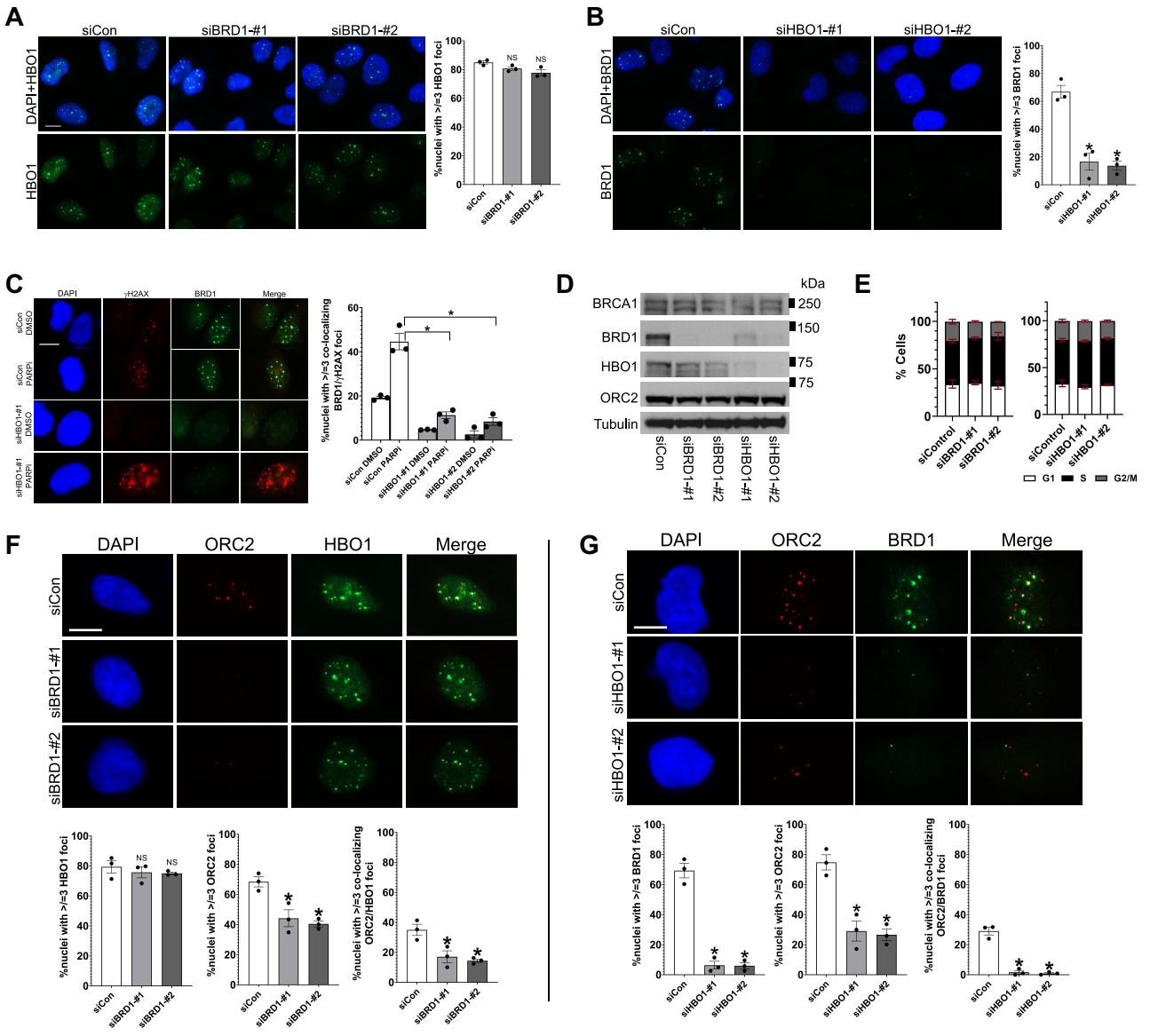

Figure 4. The BRD1–HBO1 complex promotes ORC2 localization to nuclear foci. (**A** and **B**) OVCAR8 cells were transfected with a control siRNA (siCon) and either two BRD1-specific siRNAs (siBRD1-#1 and siBRD1-#2) in (A) or two HBO1-specific siRNAs (siHBO1-#1 and siHBO1-#2) in (B), and 72 h after the first transfection were immunofluorescently stained for either HBO1 and DAPI in (A) or BRD1 and DAPI in (B). On the left in each panel are representative images of nuclei with foci. Scale bar = 10 μm. The bar graph on the right in each panel depicts the average percentage of nuclei with greater than or equal to three foci for each siRNA from three separate experiments. Error bars represent standard error of the mean. *P*-values were generated using a standard *t*-test. NS = not significant, and $*P < 0.05$ compared to the control. (**C**) OVCAR8 cells were transfected with siCon, siHBO1-#1, or siHBO1-#2. Transfected cells were then treated with either vehicle (DMSO) or 1 μM of the PARP inhibitor (PARPi) Olaparib for 24 h. Cells were then immunofluorescently stained for γH2AX and BRD1. Representative images of nuclei with foci are shown on the left. Scale bar = 10 μm. A bar graph representing the average percentage of nuclei with greater than or equal to three co-localizing foci for each siRNA from three individual experiments is shown on the right. Error bars represent standard error of the mean. *P*-values were calculated using a standard *t*-test comparing siCon to siHBO1 for each siRNA/treatment, and $*P < 0.05$. (**D**) OVCAR8 cells were transfected with siCon, two BRD1-specific siRNAs, or two HBO1-specific siRNAs, and a western blot was performed on lysates from these cells 72 h later for BRCA1, BRD1, HBO1, or ORC2 with Tubulin as a loading control. (**E**) OVCAR8 cells were transfected with a control siRNA and either two BRD1-specific siRNAs or two HBO1-specific siRNAs. 72 h later, the cells were stained for bromodeoxyuridine/propidium iodide and their cell cycle profiles analyzed by flow cytometry. The cell cycle profiles are reported in bar graphs for each treatment, with the colors of the bars representing the different cell cycle phases (G1 = white, S = black, G2/M = gray) and error bars representing standard error of the mean between three independent replicates. *P*-values were calculated using a two-way ANOVA and Dunnett's multiple comparisons test comparing siCon to either siHBO1 or siBRD1 for each cell cycle phase, and no differences were found to be significant. (**F** and **G**) OVCAR8 cells were transfected with a control siRNA and either two BRD1-specific siRNAs (F) or two HBO1-specific siRNAs (G). 72 h later, cells were immunofluorescently stained for HBO1 and ORC2 (F) or BRD1 and ORC2 (G). Representative images of nuclei with foci are shown on the top in each panel for each treatment. Bar graphs representing the average percentage of nuclei with greater than or equal to three ORC2, HBO1, or co-localizing ORC2/HBO1 foci in (F) or ORC2, BRD1, or co-localizing ORC2/BRD1 foci in (G) from three individual experiments are shown on the bottom. Error bars represent standard error of the mean. $*P < 0.05$ compared to the siCon by a standard *t*-test.

control or BRD1- or HBO1-specific inducible short hairpin RNAs (shRNAs) along with either an empty vector or full length shRNA resistant BRD1 or HBO1 respectively (Supplementary Figures S5A, S5B, S5C, S5D, S5E, S5F, S5G, S5H). Upon BRD1 and/or HBO1 depletion in the vector expressing lines, we observed a significant decrease in the percentage of nuclei with ORC2 foci compared to the control (Supplementary Figures S5D, S5H). Expression of shRNA resistant BRD1 or HBO1 restored the percentage of nuclei with ORC2 foci to levels close to the control shRNA in the setting of depletion (Supplementary Figures S5D, S5H). The changes in percentages of nuclei with ORC2 foci observed upon BRD1 or HBO1 depletion could not be attributed to significant decreases in ORC2 protein levels or cell cycle arrest, thereby validating regulation of ORC2 localization to nuclear foci as a novel role for BRD1 with HBO1 in replication origin regulation (Supplementary Figures S5A, S5B, S5E, S5F). We also again observed a decrease in BRD1 protein levels upon HBO1 depletion compared to the control that was rescued upon expression of shRNA resistant HBO1 (Supplementary Figure S5E).

Taken together, these data reveal that in an HBO1/BRD1 complex, HBO1 helps maintain BRD1 protein levels in general and in nuclear foci. Together, HBO1 and BRD1 aid in maintaining ORC2 localization to nuclear foci, a role that is unique from other BRPF family proteins (22). Given the reduction in the percentage of nuclei with HBO1/ORC2 and BRD1/ORC2 co-localizing foci in BRCA1 reconstituted UWB1.289 cells compared to the parent line (Figures 3F and H), our next question was if BRCA1 plays a direct role in regulating BRD1 and/or HBO1 at replication origins.

BRCA1, BRD1, HBO1, and BARD1 form a functional complex, ORFIUS

Based on the above findings, we hypothesized that BRD1, HBO1, and BRCA1 may form a replication origin regulatory complex. Indeed, others have shown (i) that BRCA1 is part of a larger BRD1 interactome through BRD1 affinity purification mass spectrometry (18), and (ii) that HBO1 may interact with the BRCA1 stoichiometric binding partner BARD1 through yeast two-hybrid methods (49,50). Thus, we sought to validate the existence of a BRCA1–BRD1–HBO1 complex through multiple metrics.

We first assessed for an endogenous-endogenous interaction or at least localization in close proximity of these proteins using the immunofluorescence-based protein-protein interaction detection method, proximity ligation assay (PLA), in which protein-protein interactions are represented here by nuclear foci (51). Using siRNA validated antibodies (Supplementary Figures S6A, S6B, S6C, S6D), we tested for interactions between BRCA1 and BRD1, BRCA1 and HBO1, and BRCA1 and ORC2 in FT194, OVCAR8, CaOV3, and SKOV3 cells (Figure 5A, Supplementary Figures S6E, S6F, S6G, S6H, S7). Significant interactions between BRCA1 and either BRD1, HBO1, or ORC2 were detected in all cell lines (Figure 5A, Supplementary Figures S6F, S6G, S6H). OVCAR8 cells are known to have one copy of *BRCA1* with promoter methylation and thus have lower levels of BRCA1 expression, and they had reduced numbers of PLA foci per nucleus compared to other cells for BRD1/BRCA1, HBO1/BRCA1, and ORC2/BRCA1 staining (Figure 5A) (33). Additionally, although SKOV3 showed similar average PLA foci per nucleus between BRCA1/BRD1, BRCA1/HBO1, and BRCA1/ORC2, FT194, CaOV3, and OVCAR8 all revealed less PLA foci per nucleus for BRCA1/HBO1 compared to BRCA1/BRD1 suggesting potentially a reduced interaction between these two complex members. Additionally, the two HGSC lines OVCAR8 and CaOV3 showed reduced BRCA1/ORC2 foci per nucleus compared to the SKOV3 and FT194 lines suggesting reduced BRCA1 at ORC2 marked origins in HGSC cells. These results suggest that BRCA1 interacts with or is at least in close proximity to BRD1 and HBO1 possibly at ORC2 marked origins.

Given this, we sought to further validate the existence of a BRCA1–BRD1–HBO1 complex via co-immunoprecipitation. We utilized exogenously expressed GST-tagged proteins to immunoprecipitate (IP) endogenous partners. GST was chosen because of its high affinity and lack of antibody-mediated interactions allowing for chemically strong IP of potentially transient interactions with no antibody generated background on detection western blots (52). Additionally, it is difficult to exogenously express full length BRCA1, but it is easier to exogenously express the stoichiometric BRCA1 binding partner, BARD1 (50,53). The BRCA1-BARD1 interaction has been validated by yeast two-hybrid and biochemical methods, and thus we utilized exogenously expressed GST-BARD1 as a surrogate for BRCA1 (50,53,54). We first tested for interacting partners of either full length GST-BRD1 or GST-HBO1. We found that full length GST-BRD1 IPs endogenous BRCA1, BARD1, and HBO1, while full length GST-HBO1 only IPs endogenous BRD1 (Figure 5B). We next tested for BARD1 interactions and found that full length GST-BARD1 IPs endogenous BRD1, HBO1, and BRCA1 (Figure 5C).

To help validate the IP findings, we mapped the interaction domains for BRD1 and HBO1 with their respective binding partners. BARD1 has been previously shown to interact with the BRCA1 RING domain (53). Using GST-BRD1 fragments encompassing key functional domains, we found that the bromodomain and closely surrounding region of BRD1 IPs endogenous BARD1 and BRCA1, and validated the previously shown finding that the N-terminus of BRD1 IPs endogenous HBO1 (Figure 5D) (17). Similarly, using GST-tagged fragments of HBO1 functional domains, we validated the previously shown finding that the C-terminal MYST domain of HBO1 IPs endogenous BRD1 (Figure 5E) (17,39).

Taken together, these results support that BRCA1, BRD1, HBO1, and BARD1 form a functional complex, ORigin FIring Under Stress (ORFIUS), through interaction at specific domains in each protein, a schematic of which is shown in Figure 5F. The PLA results, which support that the BRCA1, BRD1, and HBO1 interactions as part of the ORFIUS complex are physiologic, reveal a small but significant increase in the average number of PLA foci per nucleus for each interaction across cell lines compared to controls (Figure 5A). This suggests that the complex may form only under specific circumstances or transiently.

BRCA1, BRD1, and HBO1 localize together at genomic replication origin loci and ORC2 binding sites

Our next question was whether ORFIUS complex members function together at replication origins. The co-localization of BRD1 and HBO1 with ORC2 in nuclear foci likely in a BRCA1 regulated manner supports this possibility (Figures

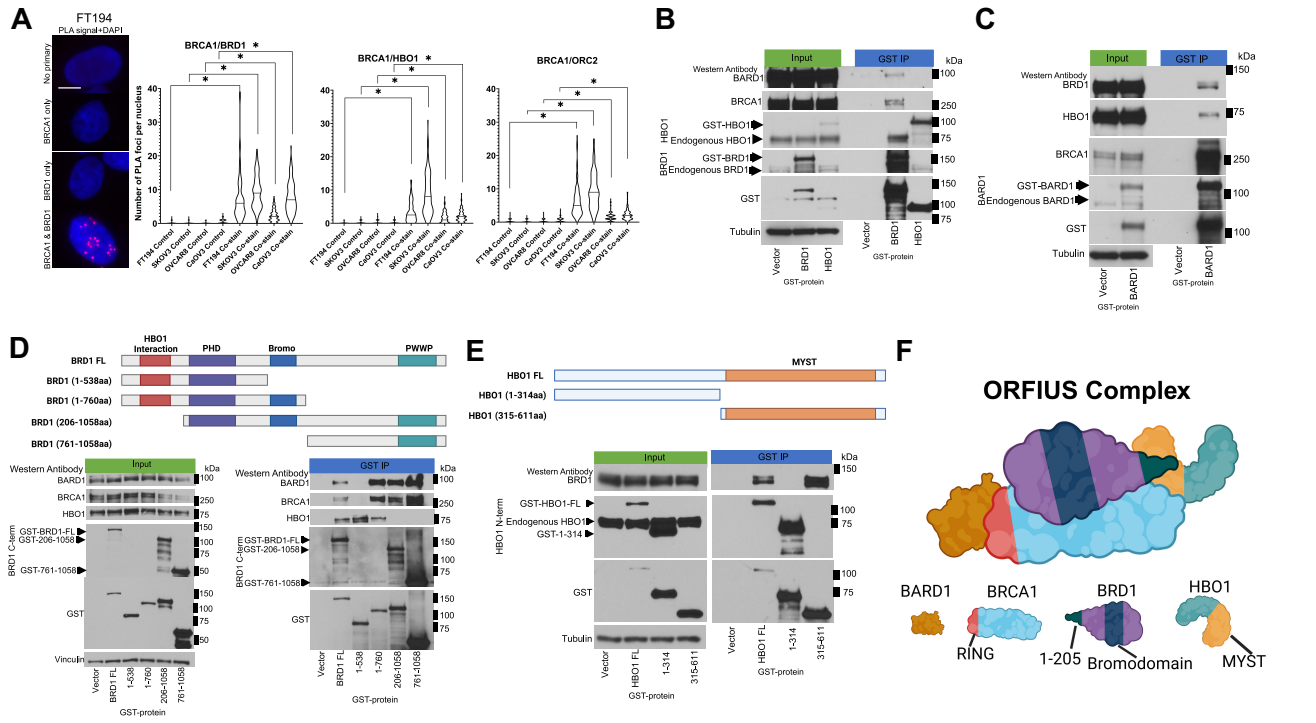

Figure 5. BRCA1, BRD1, HBO1, and BARD1 form the ORFIUS complex. (**A**) Proximity ligation assay (PLA) was performed on asynchronous FT194, OVCAR8, SKOV3, and CaOV3 cells for BRCA1 and BRD1, BRCA1 and HBO1, or BRCA1 and ORC2. Representative images of PLA foci with DAPI to mark nuclei for no antibody control, BRCA1 alone, BRD1 alone, or BRCA1-BRD1 co-stain are shown for FT194 cells on the left. Scale bars = 10 μm. Please note that these FT194 PLA signal+DAPI images are also shown in Supplementary Figure S7A along with the corresponding PLA signal alone photos, as well as representative images for all lines with this antibody pair. Violin plots from one representative experiment comparing the number of PLA foci per nucleus from at least 100 nuclei are shown for the no primary antibody control compared to the co-stain for each cell line for BRCA1-BRD1, BRCA1-HBO1, or BRCA1-ORC2 on the right. $*P < 0.05$ comparing the co-stain to the no primary antibody control by a one-way ANOVA with Tukey's multiple comparisons test. (**B–E**) 293T cells were transfected with empty vector or GST tagged full length BRD1 or HBO1 in (B), GST tagged BARD1 in (C), GST tagged full length or fragments of BRD1 in (D), or GST tagged full length or fragments of HBO1 in (E). 48 h later GST immunoprecipitations (IPs) were performed on the various lysates, and western blots were performed on the IPs. Inputs and GST IPs are shown with the western blot antibody indicated on the left and the IP target on the bottom of the blots. (Term = Terminus) For all of the experiments, expression of the GST-tagged bait is shown in a GST western for the input and IP in each panel. A green bar on top of the blots indicates input and a blue bar indicates GST IP. For westerns in which an endogenous and a GST-tagged protein may appear in the same blot, we indicate on the left side of the blot with an arrow the endogenous and the GST-tagged protein. For the fragment blots in (D) and (E), on top of the blots is a map for the respective full length and fragment proteins with key domains marked. For BRD1, domains include the N-terminus known to interact with HBO1 (HBO1 interaction), the plant homeodomain finger domain (PHD), the Bromodomain (Bromo), and the proline-tryptophan-tryptophan-proline (PWWP) domain. For HBO1, the domains include the C terminal MYST domain. FL = full length. AA = amino acids. (**F**) Schematic of ORFIUS complex interactions. On the bottom of the cartoon is a key to each protein with key functional domains indicated. For BRCA1, the N-terminal RING domain is highlighted. For BRD1, 1–205 represents the N-terminal amino acids one through 205 where HBO1 interacts. In the larger cartoon, the interactions of the four complex members are indicated at key domains in each protein based on GST IP or previously known results.

3F and H). However, to address this question and validate that our nuclear foci results do represent the function of the ORFIUS complex at replication origins, we assessed for co-occupancy of ORFIUS complex members together at genomic replication origin loci or ORC2 binding sites through chromatin immunoprecipitation sequencing (ChIP-seq). First, we analyzed publicly available ChIP-seq data for HBO1, BRCA1, and ORC2 to mark replication origins and discovered that BRCA1 and HBO1 co-occupy a subset of ORC2 marked replication origins (Figure 6A) (48,55,56). In addition, others have also shown that BRCA1 binding is enriched at a group of cell type-independent replication origins of low, medium, and high replication initiation efficiency (23).

We next addressed whether BRD1 and HBO1 co-occupy any of these ORC2 or origin sites. We performed ChIP-seq for BRD1 and HBO1 on chromatin from the parent UWB1.289 cell line, which had high levels of individual and co-localizing BRD1, HBO1, and ORC2 foci (Figures 3F and H, 6B–D, and Supplementary Figures S8A, S8B, S8C). There was overlap between BRD1 and HBO1 peaks (Figure 6B). We examined binding of BRD1 and HBO1 at either the previously reported ORC2 binding sites (Figure 6C) or cell type-independent replication origins of low, medium, or high replication initiation efficiency assessed above (Figure 6D) (23,48). We observed enriched BRD1 and HBO1 sequencing read density at the ORC2 bindings sites and the low, medium, and high efficiency origins, indicating that BRD1 and HBO1 co-occupy these origin sites (Figures 6C and D).

These ChIP-seq results support that (i) ORFIUS complex members localize to replication origins and ORC2 binding sites together, and (ii) our nuclear foci results reflect the localization and function of the complex at replication origins. Specifically, the BRD1 and HBO1 enrichment together at ORC2 binding sites and low/medium/high efficiency origin loci corresponds well with our data demonstrating co-localization of BRD1/HBO1, BRD1/ORC2, and

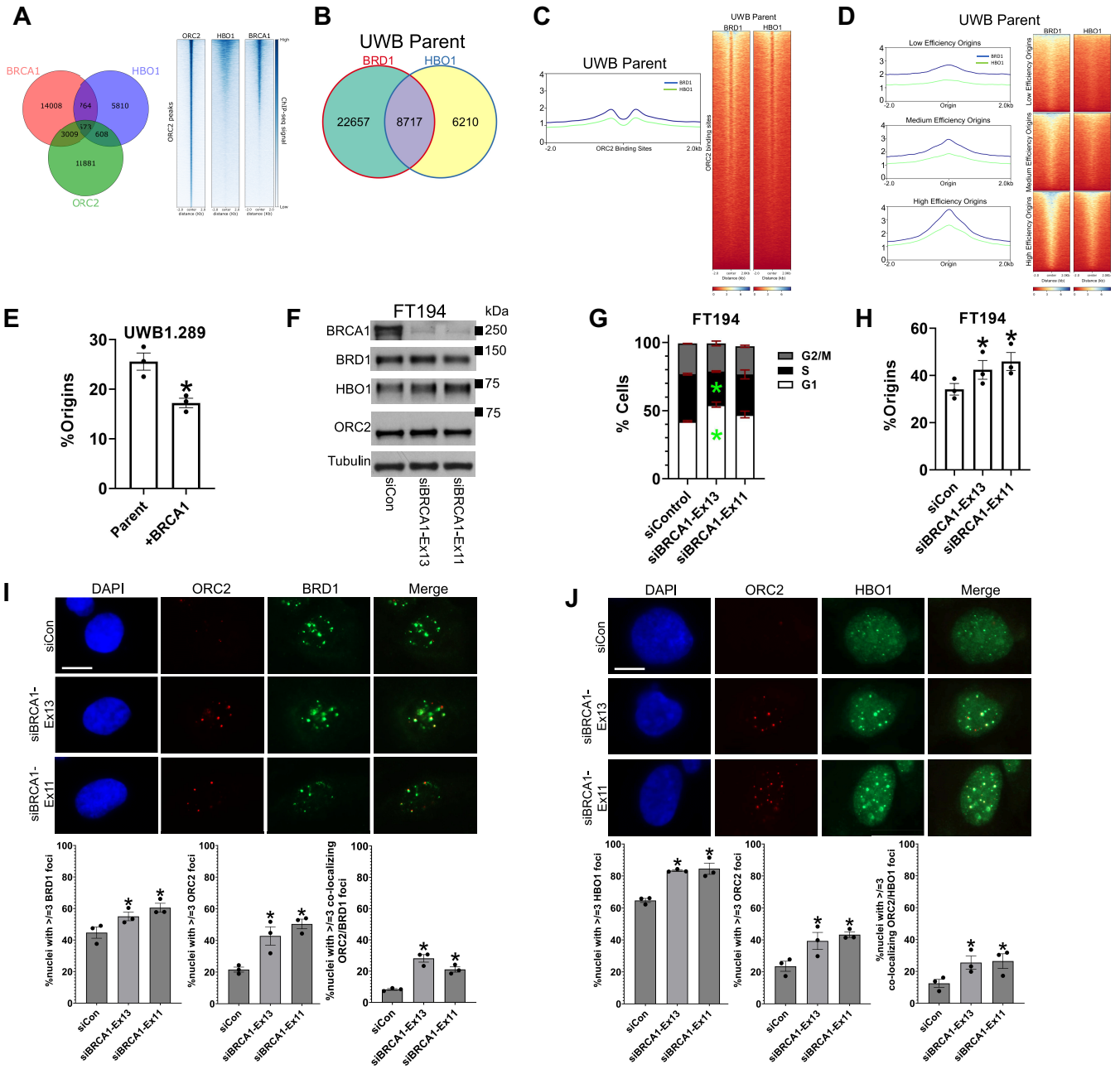

Figure 6 The ORFIUS complex localizes to replication origins and regulates ORC2 localization to nuclear foci. (**A**) Publicly available BRCA1, HBO1, or ORC2 chromatin immunoprecipitation sequencing (ChIP-seq) datasets were analyzed for co-occupancy of HBO1 and BRCA1 at origins marked by ORC2. A Venn diagram on the left shows the number of peaks exhibiting co-occupancy of the different proteins with each other, and heat maps on the right show ChIP-seq signal at ORC2 sites for the IP target on top of the graph. All overlaps between peak sets were significant ($P < 0.00001$) by permutation test. (**B–D**) BRD1 and HBO1 ChIP-seq was performed on chromatin prepared from the parental UWB1.289 cell line (UWB Parent). Two replicates per antibody were performed and analyzed. The ChIP-seq data was analyzed for (i) BRD1 and HBO1 individual and overlapping peaks, and (ii) BRD1 or HBO1 ChIP-seq read density at various publicly defined genomic regions. (B) Venn diagram demonstrating the number of BRD1 and HBO1 individual and overlapping ChIP-seq peaks for UWB1.289 parent cells. (C and D) ChIP-seq reads for BRD1 and HBO1 from UWB1.289 Parent cells were mapped to the hg38 reference genome and read density was calculated for regions identified as ORC2 binding sites in a publicly available dataset (C) or as low, medium, or high efficiency origins in a publicly available dataset (D). Profile plots demonstrating BRD1 or HBO1 read density at ORC2 (C) or origin (D) sites from one of two replicates for each antibody are shown on the left in each panel with BRD1 in blue and HBO1 in green, and heatmaps demonstrating BRD1 or HBO1 read density at ORC2 (C) or origin (D) sites for the same replicate are shown on the right in each panel. A color code of the heat map is shown at the bottom of each heat map. (**E**) Untreated UWB1.289 parent (Parent) or BRCA1 reconstituted (+BRCA1) cells were labeled for DNA fiber analysis and fibers stained. Fibers were scored to assess the percentage of firing replication origins. The bar graph represents the average percentage of firing origins from three independent experiments for each cell line. Error bars represent standard error of the mean. $^*P < 0.05$ compared to the Parent line by a standard *t*-test. (**F**) FT194 cells were transfected with a control siRNA (siCon), an siRNA against exon 13 of BRCA1 (siBRCA1-Ex13), or an siRNA against exon 11 of BRCA1 (siBRCA1-Ex11), and a western blot was performed on lysates from these cells 72 h later for BRCA1, BRD1, HBO1, or ORC2 with Tubulin as a loading control. (**G**) FT194 cells were transfected with siCon, siBRCA1-Ex13, or siBRCA1-Ex11. 72 h later, the cells were stained for bromodeoxyuridine/propidium iodide and their cell cycle profiles analyzed by flow cytometry. The cell cycle profiles are reported in bar graphs for each treatment, with the colors of the bars representing the different cell cycle phases (G1 = white, S = black, and

HBO1/ORC2 in nuclear foci (Figures 2D, 3F and H, 6A–D). The BRCA1 and HBO1 co-occupancy of ORC2 binding sites, strong overlap of BRD1 and HBO1 at the same ORC2 binding sites and low/medium/high efficiency origin loci, and known BRCA1 occupancy of the same low/medium/high efficiency origin loci corresponds with our BRD1/HBO1/ORC2 nuclear foci data and our PLA data demonstrating physiologic interactions between BRCA1/BRD1, BRCA1/HBO1, and BRCA1/ORC2 (Figures 3F and H, 5A, 6A–D).

Given this, we sought to further validate that the ORFIUS complex functions together at replication origins. We had previously observed increased percentages of nuclei with BRD1, HBO1, and ORC2 individual and co-localizing foci in the parent UWB1.289 line compared to the BRCA1 reconstituted line, which suggests that BRCA1 may regulate BRD1 and HBO1 localization to and function at replication origins as part of the ORFIUS complex (Figures 3F and H). Since we had shown that BRD1 and HBO1 promote ultimate origin firing (Figures 3B and C), we asked whether this increased origin regulatory machinery on the DNA in the absence of BRCA1 corresponds to increased replication origin firing. Indeed, using a DNA fiber assay, we found that there is significantly increased basal replication origin firing in the parent line compared to the BRCA1 reconstituted line (Figures 3A and 6E, Supplementary Figure S8D).

Taken together, these results suggest that BRCA1, BRD1, and HBO1 co-occupy at least a subset of genomic replication origin loci and/or ORC2 binding sites, where BRCA1 likely regulates localization and function of the ORFIUS complex at replication origins, and thus ultimately origin firing (Figures 6A–E).

The ORFIUS complex regulates replication origin initiation by promoting ORC2 localization to nuclear foci

Our next question was what the role of the ORFIUS complex is in replication origin regulation. Given that (i) BRD1 and HBO1 support ORC2 localization to nuclear foci (Figures 4F and G, Supplementary Figure S5), and (ii) percentages of nuclei with BRD1, HBO1 and ORC2 individual and co-localizing foci and basal origin firing are increased in the UWB1.289 parent compared to the BRCA1 reconstituted line (Figures 3F and H, 6E), we hypothesized that BRCA1 regulates replication origins by controlling BRD1 and HBO1 directed ORC2 licensing protein localization to nuclear foci. We addressed this in FT194 cells which had a reduced baseline percentage of nuclei with ORC2, BRD1, and HBO1 individual and BRD1/ORC2 and HBO1/ORC2 co-localizing foci compared to most sporadic and *BRCA1* mutant HGSC cells (Figures 3F and H).

First, we assessed whether BRCA1 depletion might lead to alterations in BRD1, HBO1, or ORC2 protein levels or significant cell cycle arrest, and found no change in any protein (Figure 6F) and that only one BRCA1 siRNA caused a small but statistically significant increase in G1 and decrease in S phase cells (Figure 6G). Next, we assessed how BRCA1 depletion affects basal origin firing by DNA fiber assay (26). We found that BRCA1 depletion leads to significantly increased replication origin firing in FT194 cells similar to the increased firing observed in the UWB1.289 parent versus BRCA1 reconstituted cells (Figures 6E and H, Supplementary Figures S8E, S8F).

Next we sought to validate that BRCA1 regulates BRD1/HBO1/ORC2 nuclear foci dynamics. In the setting of BRCA1 depletion compared to controls in FT194 cells, we observed small but statistically significant increases in both the percentage of nuclei with BRD1 and HBO1 foci, and almost a doubling or more in the percentage of nuclei with ORC2 foci and co-localizing BRD1/ORC2 and HBO1/ORC2 foci, similar to the increased foci observed in the UWB1.289 parent compared to the BRCA1 reconstituted line (Figures 3F and H, 6I and J). We did not observe these alterations in percentages of nuclei with BRD1, HBO1, or ORC2 foci upon depletion of other DNA damage repair proteins including RAD51 or ATM (Supplementary Figures S9, S10), supporting that these results are specific to BRCA1 (Figures 6H–J) (57,58).

The above results support that the ORFIUS complex regulates replication origins through BRCA1 controlling both localization of BRD1 and HBO1 to nuclear foci and BRD1/HBO1 maintenance of the ORC2 licensing protein in nuclear foci, which ultimately supports origin firing. Increased percentages of nuclei with BRD1, HBO1, and ORC2 foci in the absence of BRCA1 correspond to increased origin firing (Figures 3F and H, 6E, 6H–J), while decreased percentages of nuclei with ORC2 foci in the setting of BRD1 or HBO1 depletion correspond to decreased origin firing (Figures 3B and C, 4F and G, Supplementary Figure S5).

ORFIUS complex localization at replication origins is dysregulated in HGSC

Finally, our previous data indicates that the ORFIUS complex is dysregulated in HGSC cells. We observed an increased percentage of nuclei with BRD1/ORC2 and HBO1/ORC2 co-localizing foci and individual ORC2 foci in *BRCA1* mutant and sporadic HGSC cells compared to fallopian tube and non-HGSC ovarian cancer cell controls (Figures 3F and H). We also observed that BRD1 and HBO1 remain in nuclear foci after PARPi-induced RS in sporadic and *BRCA1* mutant HGSC cells compared to their decreasing in foci in controls (Figures 1G–I, 2E–G). This suggests that the ORFIUS complex (i) may normally regulate replication origins both at baseline and dur-

←

G2/M = gray) and error bars representing standard error of the mean between three independent replicates. *$P < 0.05$ compared to siCon for the same cell cycle phase generated by a two-way ANOVA and Dunnett's multiple comparisons test. If there is no *, the comparison is not significant. (**H**) FT194 cells were transfected with siCon, siBRCA1-Ex13, or siBRCA1-Ex11. 72 h after the first transfection, the cells were labeled for DNA fiber analysis and fibers stained. Fibers were scored to assess the percentage of firing replication origins. The bar graph represents the average percentage of firing origins from three independent experiments for each siRNA. Error bars represent standard error of the mean. *$P < 0.05$ compared to the control by a standard *t*-test. (**I** and **J**) FT194 cells were transfected with siCon, siBRCA1-Ex13, or siBRCA1-Ex11. 72 h later, cells were immunofluorescently stained for BRD1 and ORC2 (I) or HBO1 and ORC2 (J). Representative images of nuclei with foci are shown on the top in each panel for each treatment. Scale bars = 10 μm. Bar graphs representing the average percentage of nuclei with greater than or equal to three ORC2, BRD1, or co-localizing ORC2/BRD1 foci in (I) or ORC2, HBO1, or co-localizing ORC2/HBO1 foci in (J) from three individual experiments are shown on the bottom. Error bars represent standard error of the mean. *$P < 0.05$ compared to the siCon by a standard *t*-test.

ing RS, and (ii) may be inappropriately associated with replication origins promoting ORC2 localization to nuclear foci in HGSC cells regardless of origin regulatory kinase signaling or RS.

To assess this possibility, we analyzed BRD1/HBO1/ORC2 nuclear foci dynamics in non-HGSC ovarian cancer SKOV3 cells which should maintain proper replication origin regulation, OVCAR8 and CaOV3 cells to test for origin dysfunction in sporadic HGSC, and finally UWB1.289 and its BRCA1 reconstituted clone to demonstrate the BRCA1 regulatory role in the complex, all in response to inhibition of the replication origin regulatory kinases ATR and CDC7 and exposure to the RS-inducing PARPi (Figure 7A). ATR is a negative regulator of origins that should block origin firing and disengage origin machinery from DNA (24). CDC7 is a positive regulator of origins which promotes origin firing and association of origin machinery with DNA (24,26). ATR inhibition (ATRi) should promote and CDC7 inhibition (CDC7i) should block ORFIUS complex association with origins respectively (Figure 7A). PARPis should trigger ATR signaling and block association of the ORFIUS complex with origins (Figure 7A). In *BRCA1*-mutant and sporadic HGSC cells, we hypothesize that the ORFIUS complex is dysregulated and that BRD1 and HBO1 will remain associated with and promote ORC2 localization to origins, which could allow for eventual origin firing, in all of the above settings (Figure 7A).

ATR and CDC7 inhibition can induce alterations in replication origin machinery localization on DNA and firing within an hour of treatment, which can lead to increased RS over time (59). Thus, to find the best post-treatment timepoint(s) to assess RS/DNA damage- versus origin kinase inhibition-induced changes to ORFIUS nuclear foci localization, we first assessed for upregulation of RS marked by pRPA and/or DNA damage marked by γH2AX at two, eight, and 24 h post DMSO, ATRi, CDC7i, or PARPi in SKOV3 and OVCAR8 cells (Supplementary Figure S11). Post-PARPi treatment, SKOV3 and OVCAR8 cells demonstrated increased percentages of nuclei with (i) γH2AX foci at all timepoints (with smaller changes for SKOV3), (ii) pRPA foci after all timepoints, and (iii) co-localizing pRPA/γH2AX foci at all timepoints (Supplementary Figure S11). Post-ATRi treatment, both lines showed increased percentages of nuclei with pRPA foci 24 h post-treatment, and SKOV3 showed increased percentages of nuclei with co-localizing pRPA/γH2AX foci 24 h post-treatment (Supplementary Figure S11). Neither cell line revealed increased percentages of nuclei with individual or co-localizing pRPA or γH2AX foci after CDC7i treatment (Supplementary Figure S11). Based on these results, we assessed BRD1, HBO1, and ORC2 foci dynamics for all lines 24 h post treatment when (i) RS and/or RS-linked DNA damage induced nuclear foci changes due to PARPi and possibly ATRi should be strongest, and (ii) changes in origin machinery localization to nuclear foci due to ATRi and CDC7i may be strongest. We also tested a subset of cells for changes at earlier timepoints.

Before assessing complex dynamics, we examined protein levels of BRD1, HBO1, ORC2, and BRCA1 in all cell lines 24 h after all of the above treatments, and did not observe any significant alterations (Supplementary Figure S12A). We also examined cell cycle dynamics 24 h after all treatments by flow cytometry. We did not observe large arrests in SKOV3, OVCAR8, or CaOV3 with any treatment, but did observe a G1 arrest and concurrent decrease in S phase cells in both UWB1.289 parent and its BRCA1 reconstituted counterpart after ATR inhibition, along with smaller shifts with other inhibitors (Supplementary Figure S12B). These results suggest that any alterations in the percentage of nuclei with BRD1, HBO1, or ORC2 nuclear foci after any of the above treatments are (i) not due to decreased protein levels, and (ii) not likely due to large cell cycle arrests in most lines or to arrests which are not matched in a reconstituted partner for UWB1.289 cells.

Next we quantified the percentage of nuclei with co-localizing and individual BRD1, HBO1, or ORC2 foci after treatment. As expected, 24 h after treatment with ATRi, CDC7i, and PARPi compared to vehicle, the OVCAR8, CaOV3, and UWB1.289 parent lines revealed no change in the percentage of nuclei with co-localizing BRD1/ORC2, HBO1/ORC2, or BRD1/HBO1 foci or individual BRD1, HBO1, or ORC2 foci (Figures 7B–F, Supplementary Figures S12C, S13, S14, S15). For OVCAR8 cells, no changes in the percentage of nuclei with co-localizing BRD1/ORC2 or HBO1/ORC2 or individual BRD1, HBO1, or ORC2 foci were observed at two or eight h post-treatment either (Supplementary Figure S16). In contrast and as expected, 24 h post-treatment in SKOV3 cells and BRCA1 reconstituted UWB1.289 cells, we observed (i) appropriate decreases in the percentage of nuclei with BRD1/ORC2, HBO1/ORC2, and BRD1/HBO1 co-localizing and BRD1, HBO1, and ORC2 individual foci post CDC7i and PARPi treatment compared to vehicle, and (ii) appropriate increases in the percentage of nuclei with BRD1/ORC2, HBO1/ORC2, and BRD1/HBO1 co-localizing and BRD1, HBO1, and ORC2 individual foci post-ATRi treatment compared to vehicle (Figures 7B–F, Supplementary Figures S13, S14, S15). For SKOV3 cells there was a decreased percentage of nuclei with ORC2/BRD1 co-localizing and ORC2 individual foci two and eight h after PARPi treatment, and a decreased percentage of nuclei with co-localizing HBO1/ORC2 foci and individual ORC2 foci eight h post-treatment with a PARPi or CDC7i (Supplementary Figure S16).

These data, combined with our results linking BRD1, HBO1, and ORC2 foci levels to origin firing levels (Figures 3, 4, 6), support that BRCA1 regulates BRD1–HBO1 localization to origins, BRD1/HBO1 promotion of ORC2 localization in nuclear foci, and possible eventual origin firing, both at baseline and in the setting of RS. This gives the complex its name, ORFIUS. They also support that the complex is dysregulated in sporadic and *BRCA1* mutant HGSC and remains associated with and promoting ORC2 localization at origins, thus promoting possible origin firing, regardless of inhibition of origin regulatory kinases or RS.

Discussion

Genomic analysis suggests that upregulated RS or defects in the RS response may be fundamental vulnerabilities of *BRCA1* mutant and sporadic HGSCs (2). However, the critical RS suppression or response defect(s) in HGSC remains ill-defined. Here, by studying the role of the lesser known BRD-containing protein BRD1 in replication and RS, we have identified a new RS suppressing complex consisting of BRD1, HBO1, BRCA1, and BARD1, the ORFIUS complex, which regulates replication origins both at baseline and in the setting of RS (Figures 5–8). We show that BRD1 and HBO1 localize to ORC2 marked replication origins and pro-

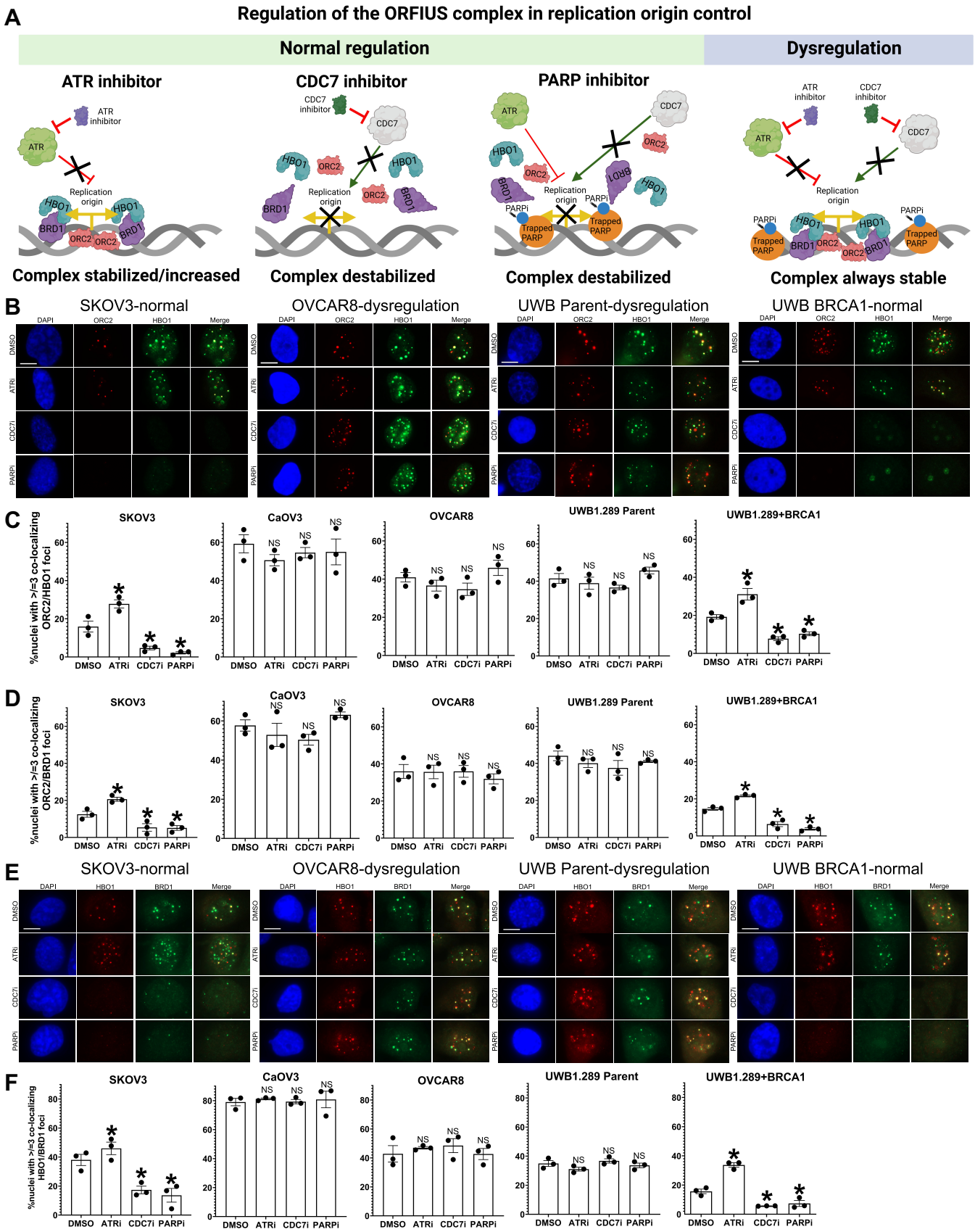

Figure 7. ORFIUS complex localization to and control of ORC2 at replication origins at baseline and during replication stress is dysregulated in *BRCA1* mutant and sporadic HGSC cells. (**A**) Cartoon representing normal regulation of BRD1, HBO1, and ORC2 at replication origins in the setting of inhibition of the origin regulatory kinases ATR or CDC7 or after PARP inhibitor (PARPi)-induced RS and/or DNA damage on the left and dysregulation of the complex in the setting of inhibition of origin regulatory kinases or RS and/or DNA damage on the right. (**B–F**) SKOV3, CaOV3, OVCAR8, UWB1.289

mote ORC2 localization in nuclear foci at baseline all in a BRCA1 regulated manner (Figures 3–6, 8). Upon depletion of BRD1 or HBO1, both origin firing and the percentage of nuclei with ORC2 foci decrease (Figures 3B and C, 4F and G, Supplementary Figure S5). Upon mutation or depletion of BRCA1, (i) the percentage of nuclei with individual or co-localizing BRD1, HBO1, and ORC2 foci increases (Figures 3F and H, 6I and J), and (ii) basal replication origin firing increases (Figures 6E and H). In the setting of RS and/or DNA damage in non-HGSC ovarian cancer cells or in BRCA1 reconstituted HGSC cells, BRD1 and HBO1 are responsive to ATR and CDC7 replication origin regulatory kinase signaling and disengage from and stop promoting ORC2 localization to nuclear foci (Figures 7, 8). The ORFIUS complex is dysregulated in *BRCA1* mutant and sporadic HGSC tumor cells. After RS or inhibition of origin regulatory kinases in these cells, BRD1 and HBO1 remain associated with origins promoting ORC2 localization in nuclear foci, likely allowing for continued strategic origin firing despite RS and/or DNA damage (Figures 7, 8). This dysregulation has both biologic and therapeutic implications in HGSC.

First, the replication origin regulatory and RS suppression roles of the ORFIUS complex are distinct from other HBO1-containing complexes, suggesting that the vulnerabilities that ORFIUS complex dysregulation create may represent a unique RS target(s) in HGSC (20,22,42). Specifically, we show that the ORFIUS complex promotes origin licensing and subsequent firing by supporting ORC2 localization to nuclear foci (Figures 3B and C, 4F and G, 6E, 6H-J, and Supplementary Figure S5). In contrast, others have shown that an HBO1-JADE1 complex supports replication origin licensing by promoting MCM2 loading, while an HBO1–BRPF3 complex supports replication origin firing by promoting CDC45 loading (20,22,42). We show here that BRPF3 does not support ORC2 localization in nuclear foci (Supplementary Figures S4E, S4F). Additionally, we show here that the ORFIUS complex helps suppress RS at baseline, as well as RS caused by agents which generate obstacles in the DNA like PARP inhibitors (Figures 1E and F, 7). In contrast, we show that the HBO1 binding partner BRPF3 does not suppress RS at baseline (Supplementary Figures S2A, S2B). However, BRPF3 has been shown to suppress RS induced by agents which cause direct fork stalling such as HU (18,22). These results suggest the mechanism of RS suppression by BRD1 is unique. Additionally, unlike other studies, our work was conducted in HGSC and HGSC precursor cells which may have unique biology and may highlight unique functions for the ORFIUS complex, as HGSC cells harbor a high level of basal DNA damage and RS. Given that other studies have shown that different binding partners direct HBO1 histone tail specificity and thus HBO1 complex function, it is not surprising that we have found roles that are distinct for the ORFIUS complex from other HBO1-containing complexes (60). Dysfunction or dysregulation of different HBO1-containing complexes may create different defects that may be differentially targeted in HGSC or other cancer cells. Further dissecting the unique role of the ORFIUS complex in basal replication origin regulation, RS, and ovarian or other cancer biology along with the consequences of its dysregulation compared to other HBO1 complexes will be an exciting area of future investigation. Furthermore, it will also be important in the future to determine if any other proteins support the origin regulatory function of the ORFIUS complex, such as known HBO1-BRD1 interacting proteins like ING4 amongst others (19).

Additionally, unlike other BRPF family members, we have found that BRD1 interacts with and is regulated by BRCA1 as part of the OFRIUS complex (Figures 5 and 6, and (18)). This raises the possibility that ORFIUS complex dysregulation could be a marker of '*BRCA*ness' in HGSC. Although the majority of HGSCs are sporadic and *BRCA1* wildtype, it is hypothesized that there are sporadic '*BRCA1*-like' HGSCs with functional defects in *BRCA1*-related pathways which may be sensitive to therapies targeting *BRCA1* pathway defects (2). The exact BRCA1-linked defect(s) and thus marker(s) of *BRCA*ness in HGSC or other BRCA1-linked cancers has not been identified. Based on our findings of dysregulated ORFIUS complex origin regulation in both sporadic and *BRCA1* mutant HGSCs, it is possible that ORFIUS dysregulation may be a marker of *BRCA*ness in some sporadic HGSCs (Figures 7B–F). Verifying this possibility through assessment of replication origin control, ORFIUS complex function, and sensitivity to therapies targeting *BRCA1* functional defects in a larger number of HGSC cell lines and primary cells of different genetic backgrounds is an important area of future investigation, as it may have biologic and therapeutic implications for some sporadic HGSCs.

Also, ORFIUS complex dysregulation may be a pathway for transition of ovarian cancer precursor cells to malignancy. HGSCs may arise from the ovarian surface epithelium, peritoneum, or fallopian tube secretory epithelium (61). Here, we show that BRD1-HBO1-ORC2 localization at replication origins is only upregulated in ovarian cancer cells and not in FT-SEC precursors (Figures 3F and H). This suggests the possibility that dysregulation of the ORFIUS complex may be a transformative event in HGSC development which, although beyond the scope of this work, merits further investigation.

Additionally, ORFIUS complex origin control dysregulation is a potential therapeutic target. We show that the BRD1 and HBO1 ORFIUS complex members are both widely expressed and survival promoting proteins in ovarian cancer (Figures 1A and C, 2A and B), and that the ORFIUS complex is dysregulated in HGSC (Figure 7). Thus, ORFIUS complex members may be reasonable single agent RS targets in HGSC. Additionally, ORFIUS complex dysregulation may alter sensitivity to RS therapies which utilize replication origin control to induce cytotoxicity, including ATR, CHK1, and PARP

parent, and the BRCA1 reconstituted version of UWB1.289 (UWB1.289 + BRCA1) were treated with vehicle (DMSO), 1 μM of the ATR inhibitor AZD6738 (ATRi), 1 μM of the CDC7 inhibitor XL-413 (CDC7i), or 1 μM of the PARP inhibitor Olaparib (PARPi) for 24 h. The cells were then immunofluorescently stained for ORC2 and HBO1 (B and C), ORC2 and BRD1 (D), or BRD1 and HBO1 (E and F). Representative images of SKOV3, OVCAR8, UWB1.289 parent (UWB Parent), and UWB1.289 + BRCA1 (UWB BRCA1) nuclei with foci are shown in (B) for ORC2/HBO1 and (E) for BRD1/HBO1, with complex regulation status for the specific line indicated above the images (normal versus dysregulation). Scale bar = 10 μm. A bar graph representing the average percentage of nuclei with greater than or equal to three co-localizing foci for each staining pattern for each treatment from three individual experiments is shown in (C) for ORC2/HBO1, (D) for ORC2/BRD1, and (F) for BRD1/HBO1. Error bars represent standard error of the mean. *P*-values were calculated using a one-way ANOVA with Dunnett's multiple comparison test, and $*P < 0.05$ compared to DMSO. NS = not significant compared to DMSO.

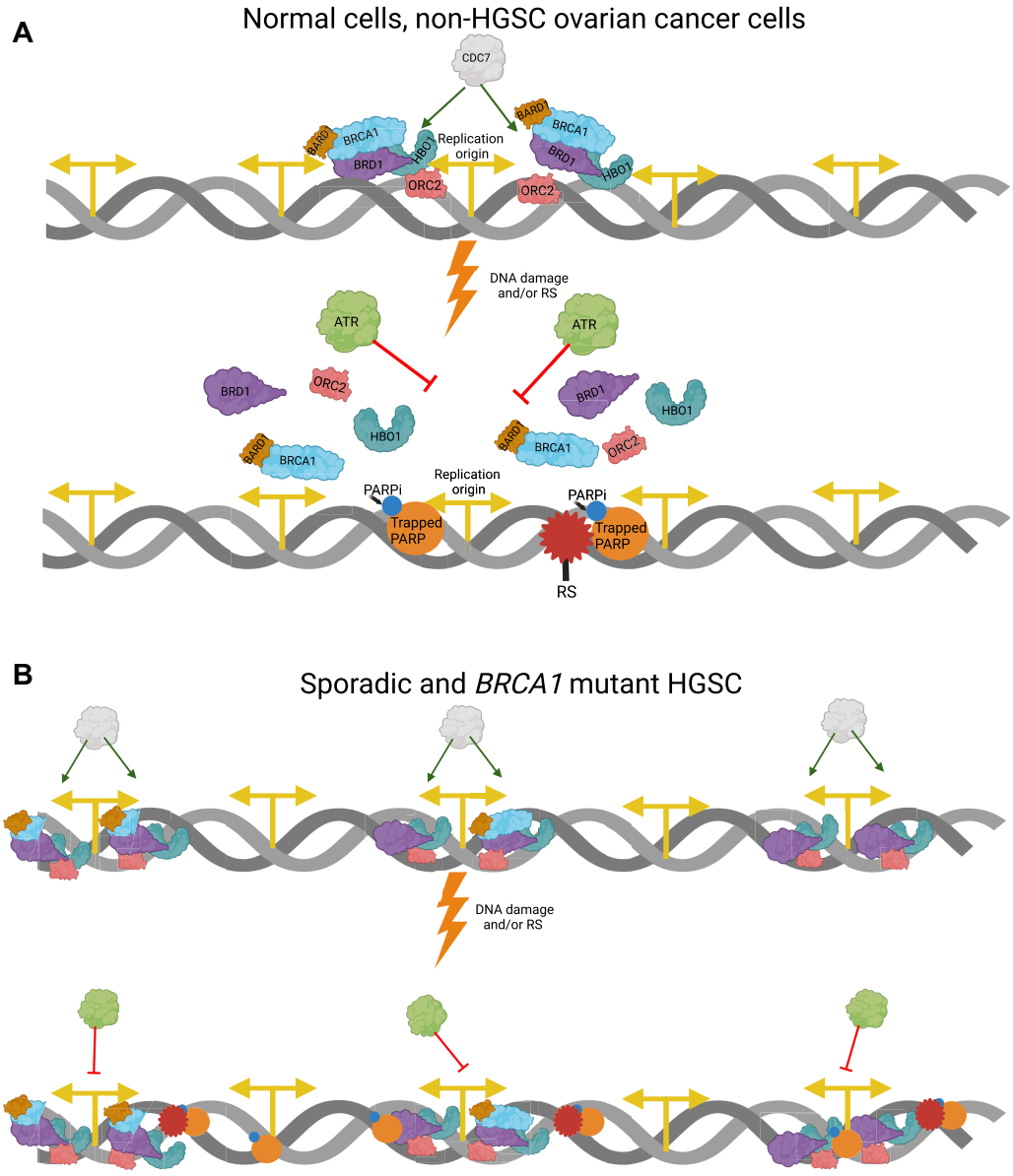

Figure 8. Models for ORFIUS complex function at replication origins in different settings. (**A**) Model for ORFIUS complex function in normal and non-HGSC ovarian cancer cells. At baseline BRCA1 regulates BRD1-HBO1 localization to and promotion of ORC2 localization at replication origins. The complex is responsive to CDC7 kinase regulation of origins. In the setting of DNA damage and/or replication stress (RS) induced by agents like PARP inhibitors (PARPi), ATR signaling is activated, and in response the ORFIUS complex dissociates from replication origins and no longer promotes ORC2 localization there. (**B**) Model for ORFIUS complex function in *BRCA1* mutant and sporadic (*BRCA1* wildtype) HGSC cells. In *BRCA1* mutant HGSC cells, either a BRCA1 truncation or point mutant or no BRCA1 may be expressed, or in sporadic HGSC cells full length BRCA1 may be expressed but signaling may be altered. In each case, BRCA1 control of HBO1, BRD1, and ORC2 at origins may be dysfunctional. There is more ORFIUS complex associated with origins than in non-malignant or non-HGSC ovarian cancer cells promoting ORC2 localization there at baseline. In the setting of DNA damage and/or RS, the ORFIUS complex is not responsive to ATR signaling and remains associated with origins promoting ORC2 localization there.

inhibitors (28,59). Thus, ORFIUS complex combination therapy strategies with these agents may also be important RS targeting possibilities in HGSC. In support of this, CDC7 origin regulatory kinase inhibitors have shown *in vivo* synergy with PARPis in certain HGSC models suggesting that targeting replication origin regulatory machinery may increase sensitivity to other RS therapies in some HGSC genetic backgrounds (62). Both BRD1 and HBO1 harbor chemically targetable protein domains, a BRD for BRD1 and an acetyltransferase domain for HBO1, making both proteins potential therapeutic targets. There are limited small molecules available for either protein, and none have been tested thoroughly for target specificity or tumor cell cytotoxicity in HGSC (63,64). An important future direction will be to develop small molecules able to engage these two ORFIUS complex proteins in HGSC, and to determine which if any current RS agents ORFIUS complex therapies may therapeutically and mechanistically synergize with.

Finally, key to the biologic discoveries in this work and their many implications was our utilization of fluorescence microscopy to study localization dynamics of BRD1, HBO1, and ORC2, which has not been done before. Previous stud-

ies have linked HBO1/BRD protein complexes to replication origins using chromatin immunoprecipitation, but did not examine dynamics of the complex across different cancer cell genotypes amid different treatments (20,22,42). Other studies have linked BET family BRD proteins indirectly to RS and/or DDR through various functions in transcription regulation, but did not examine nuclear localization of the BRD proteins (12–15). Here, our use of fluorescence microscopy to study BRD1, HBO1, and ORC2 in multiple ovarian cancer genotypes after multiple origin perturbing treatments allowed us to visualize the advantageous dysregulation of replication origin control by this complex in HGSC cells (Figures 1G–I, 2D–G, 3F and H, 7B–F). Others have suggested that analyzing replication fork dynamics in patient tumor samples or patient-derived HGSC organoids through DNA fiber assays may provide biomarkers for response to specific RS therapies (29,65). Based on our immunofluorescence work here, we propose that an important area for future translational investigation which is beyond the scope of this work will be to explore correlations between (i) RS therapy sensitivity, and (ii) BRD1, HBO1, and ORC2 nuclear foci quantity/dynamics as a marker of replication origin regulatory capacity in patient tumor samples or organoid models. This may offer insight into whether ORFIUS complex dysfunction marked by nuclear foci could serve as a biomarker for response or resistance to certain RS therapies (e.g. ATR inhibitors).

Overall, the work in this study has revealed the existence of the ORFIUS complex and defined its role in regulating replication origins at baseline and during RS through control of the origin licensing protein ORC2. ORFIUS complex replication origin control is an exciting area for continued investigation as both a possible defining defect in ovarian carcinogenesis and HGSC biology, as well as a broad RS therapeutic target in this lethal malignancy.

Data availability

All raw FCS files for flow cytometry data presented in the Main and Supplementary Figures are available in the Dryad Digital Repository at https://doi.org/10.5061/dryad.sn02v6x89. ChIP-seq data presented in Figures 6B, 6C, and 6D are available at GEO accession number GSE244027. The genome browser session for this data can be viewed by opening https://genome.ucsc.edu/cgi-bin/hgHubConnect, clicking on the "Connected Hubs" tab, pasting ftp://ftp.dfci.harvard.edu/pub/helena/hub.txt into the URL text box, and clicking "Add Hub." Next, click on the blue "Go" button on the UCSC Genome Browser page that opens. On the next page that opens, scroll down to see the tracks for this data. All other raw data presented in this article are available upon request to the corresponding author.

Supplementary data

Supplementary Data are available at NAR Cancer Online.

Acknowledgements

This manuscript is dedicated to the extraordinary Dr. David M. Livingston, a 20-year mentor to S.J.H. Thank you for the endless support and encouragement, the ability and courage to ask the toughest questions, and a lifetime of wonderful memories. I will keep chasing the mysteries of BRCA1 with you always present in spirit.

The authors gratefully acknowledge James A. DeCaprio, David E. Hill, and Myles Brown (DFCI) for helpful discussions.

The Graphical Abstract, Figure 8, and portions of Figures 1, 3, 5, and 7 were created with BioRender.com.

Author contributions: S.J.H. conceived of the project, designed, executed, and analyzed all experiments, and wrote and edited the manuscript. Z.Y. designed, executed, and analyzed all experiments. S.M. cloned all plasmids in Figure 5 and Supplementary Figure S5, performed data analysis, and aided in experimental execution. R.H. performed chromatin immunoprecipitation sequencing analysis for Figure 6A. E.L.B. and S.J.HS. performed chromatin immunoprecipitation sequencing analysis in Figures 6B, 6C, and 6D. All authors reviewed and edited the manuscript.

Funding

S.J.H was supported by a DOD OCRP Pilot Award (W81XWH-19-1-0123), a Tina's Wish Rising Star Grant, an NIH Director's Early Independence Award (DP5 OD029637), a DOD PRCRP Impact Award (W81XWH-22-1-0269), and 2021 and 2022 Dana-Farber Cancer Institute Medical Oncology Grants Program Awards. Z.Y. was supported by an OCRA Mentored Investigator Fellowship. S.M. was supported by a Helen Gurley Brown Presidential Initiative Fellowship from the Helen Gurley Brown Foundation.

Conflict of interest statement

S.J.H. receives sponsored research support from Eli Lilly and Company and Merck, Sharp & Dohme Corporation and previously received support from AstraZeneca. None is directly related to this work. All other authors have nothing to report.

References

1. Narod,S. (2016) Can advanced-stage ovarian cancer be cured?*Nat. Rev. Clin. Oncol.*, **13**, 255–261.
2. Cancer Genome Atlas Research, N. (2011) Integrated genomic analyses of ovarian carcinoma. *Nature*, **474**, 609–615.
3. Zeman,M.K. and Cimprich,K.A. (2014) Causes and consequences of replication stress. *Nat. Cell Biol.*, **16**, 2–9.
4. da Costa,A., Chowdhury,D., Shapiro,G.I., D'Andrea,A.D. and Konstantinopoulos,P.A. (2023) Targeting replication stress in cancer therapy. *Nat. Rev. Drug Discov.*, **22**, 38–58.
5. Cortez,D. (2015) Preventing replication fork collapse to maintain genome integrity. *DNA Repair (Amst.)*, **32**, 149–157.
6. Karst,A.M., Jones,P.M., Vena,N., Ligon,A.H., Liu,J.F., Hirsch,M.S., Etemadmoghadam,D., Bowtell,D.D. and Drapkin,R. (2014) Cyclin E1 deregulation occurs early in secretory cell transformation to promote formation of fallopian tube-derived high-grade serous ovarian cancers. *Cancer Res.*, **74**, 1141–1152.
7. Schlacher,K., Wu,H. and Jasin,M. (2012) A distinct replication fork protection pathway connects Fanconi anemia tumor suppressors to RAD51-BRCA1/2. *Cancer Cell*, **22**, 106–116.
8. Baxter,J.S., Zatreanu,D., Pettitt,S.J. and Lord,C.J. (2022) Resistance to DNA repair inhibitors in cancer. *Mol. Oncol*, **16**, 3811–3827.
9. Konstantinopoulos,P.A., Lee,J.M., Gao,B., Miller,R., Lee,J.Y., Colombo,N., Vergote,I., Credille,K.M., Young,S.R., McNeely,S., *et al.* (2022) A Phase 2 study of prexasertib (LY2606368) in

platinum resistant or refractory recurrent ovarian cancer. *Gynecol Oncol*, **167**, 213–225.
10. Konstantinopoulos,P.A., da Costa,A., Gulhan,D., Lee,E.K., Cheng,S.C., Hendrickson,A.E.W., Kochupurakkal,B., Kolin,D.L., Kohn,E.C., Liu,J.F., *et al.* (2021) A Replication stress biomarker is associated with response to gemcitabine versus combined gemcitabine and ATR inhibitor therapy in ovarian cancer. *Nat. Commun.*, **12**, 5574.
11. Fujisawa,T. and Filippakopoulos,P. (2017) Functions of bromodomain-containing proteins and their roles in homeostasis and cancer. *Nat. Rev. Mol. Cell Biol.*, **18**, 246–262.
12. Yang,L., Zhang,Y., Shan,W., Hu,Z., Yuan,J., Pi,J., Wang,Y., Fan,L., Tang,Z., Li,C., *et al.* (2017) Repression of BET activity sensitizes homologous recombination-proficient cancers to PARP inhibition. *Sci. Transl. Med.*, **9**, eaal1645.
13. Sun,C., Yin,J., Fang,Y., Chen,J., Jeong,K.J., Chen,X., Vellano,C.P., Ju,Z., Zhao,W., Zhang,D., *et al.* (2018) BRD4 inhibition is synthetic lethal with PARP inhibitors through the induction of homologous recombination deficiency. *Cancer Cell*, **33**, 401–416.
14. Karakashev,S., Zhu,H., Yokoyama,Y., Zhao,B., Fatkhutdinov,N., Kossenkov,A.V., Wilson,A.J., Simpkins,F., Speicher,D., Khabele,D., *et al.* (2017) BET bromodomain inhibition synergizes with PARP inhibitor in epithelial ovarian cancer. *Cell Rep.*, **21**, 3398–3405.
15. Lam,F.C., Kong,Y.W., Huang,Q., Vu Han,T.L., Maffa,A.D., Kasper,E.M. and Yaffe,M.B. (2020) BRD4 prevents the accumulation of R-loops and protects against transcription-replication collision events and DNA damage. *Nat. Commun.*, **11**, 4083.
16. McCullagh,P., Chaplin,T., Meerabux,J., Grenzelias,D., Lillington,D., Poulsom,R., Gregorini,A., Saha,V. and Young,B.D. (1999) The cloning, mapping and expression of a novel gene, BRL, related to the AF10 leukaemia gene. *Oncogene*, **18**, 7442–7452.
17. Mishima,Y., Miyagi,S., Saraya,A., Negishi,M., Endoh,M., Endo,T.A., Toyoda,T., Shinga,J., Katsumoto,T., Chiba,T., *et al.* (2011) The Hbo1-Brd1/Brpf2 complex is responsible for global acetylation of H3K14 and required for fetal liver erythropoiesis. *Blood*, **118**, 2443–2453.
18. Kim,J.J., Lee,S.Y., Gong,F., Battenhouse,A.M., Boutz,D.R., Bashyal,A., Refvik,S.T., Chiang,C.M., Xhemalce,B., Paull,T.T., *et al.* (2019) Systematic bromodomain protein screens identify homologous recombination and R-loop suppression pathways involved in genome integrity. *Genes Dev.*, **33**, 1751–1774.
19. Avvakumov,N. and Cote,J. (2007) The MYST family of histone acetyltransferases and their intimate links to cancer. *Oncogene*, **26**, 5395–5407.
20. Miotto,B. and Struhl,K. (2008) HBO1 histone acetylase is a coactivator of the replication licensing factor Cdt1. *Genes Dev.*, **22**, 2633–2638.
21. Niida,H., Matsunuma,R., Horiguchi,R., Uchida,C., Nakazawa,Y., Motegi,A., Nishimoto,K., Sakai,S., Ohhata,T., Kitagawa,K., *et al.* (2017) Phosphorylated HBO1 at UV irradiated sites is essential for nucleotide excision repair. *Nat. Commun.*, **8**, 16102.
22. Feng,Y., Vlassis,A., Roques,C., Lalonde,M.E., Gonzalez-Aguilera,C., Lambert,J.P., Lee,S.B., Zhao,X., Alabert,C., Johansen,J.V., *et al.* (2016) BRPF3-HBO1 regulates replication origin activation and histone H3K14 acetylation. *EMBO J.*, **35**, 176–192.
23. Murat,P., Perez,C., Crisp,A., van Eijk,P., Reed,S.H., Guilbaud,G. and Sale,J.E. (2022) DNA replication initiation shapes the mutational landscape and expression of the human genome. *Sci. Adv.*, **8**, eadd3686.
24. Saldivar,J.C., Cortez,D. and Cimprich,K.A. (2017) The essential kinase ATR: ensuring faithful duplication of a challenging genome. *Nat. Rev. Mol. Cell Biol.*, **18**, 622–636.
25. Boos,D. and Ferreira,P. (2019) Origin firing regulations to control genome replication timing. *Genes (Basel)*, **10**, 199.
26. Suski,J.M., Ratnayeke,N., Braun,M., Zhang,T., Strmiska,V., Michowski,W., Can,G., Simoneau,A., Snioch,K., Cup,M., *et al.* (2022) CDC7-independent G1/S transition revealed by targeted protein degradation. *Nature*, **605**, 357–365.
27. Heller,R.C., Kang,S., Lam,W.M., Chen,S., Chan,C.S. and Bell,S.P. (2011) Eukaryotic origin-dependent DNA replication in vitro reveals sequential action of DDK and S-CDK kinases. *Cell*, **146**, 80–91.
28. Simoneau,A., Xiong,R. and Zou,L. (2021) The trans cell cycle effects of PARP inhibitors underlie their selectivity toward BRCA1/2-deficient cells. *Genes Dev.*, **35**, 1271–1289.
29. Hill,S.J., Decker,B., Roberts,E.A., Horowitz,N.S., Muto,M.G., Worley,M.J. Jr, Feltmate,C.M., Nucci,M.R., Swisher,E.M., Nguyen,H., *et al.* (2018) Prediction of DNA repair inhibitor response in short-term patient-derived ovarian cancer organoids. *Cancer Discov.*, **8**, 1404–1421.
30. Schwab,R.A. and Niedzwiedz,W. (2011) Visualization of DNA replication in the vertebrate model system DT40 using the DNA fiber technique. *J. Vis. Exp.*, **56**, e3255.
31. Domcke,S., Sinha,R., Levine,D.A., Sander,C. and Schultz,N. (2013) Evaluating cell lines as tumour models by comparison of genomic profiles. *Nat. Commun.*, **4**, 2126.
32. DelloRusso,C., Welcsh,P.L., Wang,W., Garcia,R.L., King,M.C. and Swisher,E.M. (2007) Functional characterization of a novel BRCA1-null ovarian cancer cell line in response to ionizing radiation. *Mol. Cancer Res.*, **5**, 35–45.
33. Kondrashova,O., Topp,M., Nesic,K., Lieschke,E., Ho,G.Y., Harrell,M.I., Zapparoli,G.V., Hadley,A., Holian,R., Boehm,E., *et al.* (2018) Methylation of all BRCA1 copies predicts response to the PARP inhibitor rucaparib in ovarian carcinoma. *Nat. Commun.*, **9**, 3970.
34. Anglesio,M.S., Wiegand,K.C., Melnyk,N., Chow,C., Salamanca,C., Prentice,L.M., Senz,J., Yang,W., Spillman,M.A., Cochrane,D.R., *et al.* (2013) Type-specific cell line models for type-specific ovarian cancer research. *PLoS One*, **8**, e72162.
35. Karst,A.M. and Drapkin,R. (2012) Primary culture and immortalization of human fallopian tube secretory epithelial cells. *Nat. Protoc.*, **7**, 1755–1764.
36. Perets,R., Wyant,G.A., Muto,K.W., Bijron,J.G., Poole,B.B., Chin,K.T., Chen,J.Y., Ohman,A.W., Stepule,C.D., Kwak,S., *et al.* (2013) Transformation of the fallopian tube secretory epithelium leads to high-grade serous ovarian cancer in Brca;Tp53;Pten models. *Cancer Cell*, **24**, 751–765.
37. Hill,S.J., Clark,A.P., Silver,D.P. and Livingston,D.M. (2014) BRCA1 pathway function in basal-like breast cancer cells. *Mol. Cell. Biol.*, **34**, 3828–3842.
38. Gong,F., Chiu,L.Y., Cox,B., Aymard,F., Clouaire,T., Leung,J.W., Cammarata,M., Perez,M., Agarwal,P., Brodbelt,J.S., *et al.* (2015) Screen identifies bromodomain protein ZMYND8 in chromatin recognition of transcription-associated DNA damage that promotes homologous recombination. *Genes Dev.*, **29**, 197–211.
39. Tao,Y., Zhong,C., Zhu,J., Xu,S. and Ding,J. (2017) Structural and mechanistic insights into regulation of HBO1 histone acetyltransferase activity by BRPF2. *Nucleic Acids Res.*, **45**, 5707–5719.
40. Iizuka,M. and Stillman,B. (1999) Histone acetyltransferase HBO1 interacts with the ORC1 subunit of the human initiator protein. *J. Biol. Chem.*, **274**, 23027–23034.
41. Burke,T.W., Cook,J.G., Asano,M. and Nevins,J.R. (2001) Replication factors MCM2 and ORC1 interact with the histone acetyltransferase HBO1. *J. Biol. Chem.*, **276**, 15397–15408.
42. Miotto,B. and Struhl,K. (2010) HBO1 histone acetylase activity is essential for DNA replication licensing and inhibited by Geminin. *Mol. Cell*, **37**, 57–66.
43. Wang,Y., Chen,S., Tian,W., Zhang,Q., Jiang,C., Qian,L. and Liu,Y. (2019) High-expression HBO1 predicts poor prognosis in gastric cancer. *Am. J. Clin. Pathol.*, **152**, 517–526.
44. Zhong,W., Liu,H., Deng,L., Chen,G. and Liu,Y. (2021) HBO1 overexpression is important for hepatocellular carcinoma cell growth. *Cell Death. Dis.*, **12**, 549.

45. Chen,Z., Zhou,L., Wang,L., Kazobinka,G., Zhang,X., Han,X., Li,B. and Hou,T. (2018) HBO1 promotes cell proliferation in bladder cancer via activation of Wnt/beta-catenin signaling. *Mol. Carcinog.*, **57**, 12–21.
46. Kueh,A.J., Eccles,S., Tang,L., Garnham,A.L., May,R.E., Herold,M.J., Smyth,G.K., Voss,A.K. and Thomas,T. (2020) HBO1 (KAT7) does not have an essential role in cell proliferation, DNA replication, or histone 4 acetylation in human cells. *Mol. Cell. Biol.*, **40**, e00506-19.
47. Quinet,A., Carvajal-Maldonado,D., Lemacon,D. and Vindigni,A. (2017) DNA fiber analysis: mind the Gap!. *Methods Enzymol.*, **591**, 55–82.
48. Miotto,B., Ji,Z. and Struhl,K. (2016) Selectivity of ORC binding sites and the relation to replication timing, fragile sites, and deletions in cancers. *Proc. Natl. Acad. Sci. U.S.A.*, **113**, E4810–E4819.
49. Goehler,H., Lalowski,M., Stelzl,U., Waelter,S., Stroedicke,M., Worm,U., Droege,A., Lindenberg,K.S., Knoblich,M., Haenig,C., *et al.* (2004) A protein interaction network links GIT1, an enhancer of huntingtin aggregation, to Huntington's disease. *Mol. Cell*, **15**, 853–865.
50. Hill,S.J., Rolland,T., Adelmant,G., Xia,X., Owen,M.S., Dricot,A., Zack,T.I., Sahni,N., Jacob,Y., Hao,T., *et al.* (2014) Systematic screening reveals a role for BRCA1 in the response to transcription-associated DNA damage. *Genes Dev.*, **28**, 1957–1975.
51. Gomes,I., Sierra,S. and Devi,L.A. (2016) Detection of receptor heteromerization using in situ proximity ligation assay. *Curr. Protoc. Pharmacol.*, **75**, 2.16.1–2.16.31.
52. Kaelin,W.G. Jr, Pallas,D.C., DeCaprio,J.A., Kaye,F.J. and Livingston,D.M. (1991) Identification of cellular proteins that can interact specifically with the T/E1A-binding region of the retinoblastoma gene product. *Cell*, **64**, 521–532.
53. Brzovic,P.S., Rajagopal,P., Hoyt,D.W., King,M.C. and Klevit,R.E. (2001) Structure of a BRCA1-BARD1 heterodimeric RING-RING complex. *Nat. Struct. Biol.*, **8**, 833–837.
54. Greenberg,R.A., Sobhian,B., Pathania,S., Cantor,S.B., Nakatani,Y. and Livingston,D.M. (2006) Multifactorial contributions to an acute DNA damage response by BRCA1/BARD1-containing complexes. *Genes Dev.*, **20**, 34–46.
55. Xiao,Y., Li,W., Yang,H., Pan,L., Zhang,L., Lu,L., Chen,J., Wei,W., Ye,J., Li,J., *et al.* (2021) HBO1 is a versatile histone acyltransferase critical for promoter histone acylations. *Nucleic Acids Res.*, **49**, 8037–8059.
56. Pope,B.D., Ryba,T., Dileep,V., Yue,F., Wu,W., Denas,O., Vera,D.L., Wang,Y., Hansen,R.S., Canfield,T.K., *et al.* (2014) Topologically associating domains are stable units of replication-timing regulation. *Nature*, **515**, 402–405.
57. Jeggo,P.A. and Lobrich,M. (2006) Contribution of DNA repair and cell cycle checkpoint arrest to the maintenance of genomic stability. *DNA Repair (Amst.)*, **5**, 1192–1198.
58. O'Donovan,P.J. and Livingston,D.M. (2010) BRCA1 and BRCA2: breast/ovarian cancer susceptibility gene products and participants in DNA double-strand break repair. *Carcinogenesis*, **31**, 961–967.
59. Moiseeva,T., Hood,B., Schamus,S., O'Connor,M.J., Conrads,T.P. and Bakkenist,C.J. (2017) ATR kinase inhibition induces unscheduled origin firing through a Cdc7-dependent association between GINS and And-1. *Nat. Commun.*, **8**, 1392.
60. Lalonde,M.E., Avvakumov,N., Glass,K.C., Joncas,F.H., Saksouk,N., Holliday,M., Paquet,E., Yan,K., Tong,Q., Klein,B.J., *et al.* (2013) Exchange of associated factors directs a switch in HBO1 acetyltransferase histone tail specificity. *Genes Dev.*, **27**, 2009–2024.
61. Kroeger,P.T. Jr and Drapkin,R. (2017) Pathogenesis and heterogeneity of ovarian cancer. *Curr. Opin. Obstet. Gynecol.*, **29**, 26–34.
62. Iwai,K., Nambu,T., Kashima,Y., Yu,J., Eng,K., Miyamoto,K., Kakoi,K., Gotou,M., Takeuchi,T., Kogame,A., *et al.* (2021) A CDC7 inhibitor sensitizes DNA-damaging chemotherapies by suppressing homologous recombination repair to delay DNA damage recovery. *Sci. Adv.*, **7**, eabf0197.
63. Gao,Y.Y., Ling,Z.Y., Zhu,Y.R., Shi,C., Wang,Y., Zhang,X.Y., Zhang,Z.Q., Jiang,Q., Chen,M.B., Yang,S., *et al.* (2021) The histone acetyltransferase HBO1 functions as a novel oncogenic gene in osteosarcoma. *Theranostics*, **11**, 4599–4615.
64. Bouche,L., Christ,C.D., Siegel,S., Fernandez-Montalvan,A.E., Holton,S.J., Fedorov,O., Ter Laak,A., Sugawara,T., Stockigt,D., Tallant,C., *et al.* (2017) Benzoisoquinolinediones as potent and selective inhibitors of BRPF2 and TAF1/TAF1L bromodomains. *J. Med. Chem.*, **60**, 4002–4022.
65. Yazinski,S.A., Comaills,V., Buisson,R., Genois,M.M., Nguyen,H.D., Ho,C.K., Todorova Kwan,T., Morris,R., Lauffer,S., Nussenzweig,A., *et al.* (2017) ATR inhibition disrupts rewired homologous recombination and fork protection pathways in PARP inhibitor-resistant BRCA-deficient cancer cells. *Genes Dev.*, **31**, 318–332.